Research Repository UCD

Title	Ensemble Calibration of Lumped Parameter Retrofit Building Models using Particle Swarm Optimization
Authors(s)	Andrade-Cabrera, Carlos, Burke, Daniel J., Turner, William J. N., Finn, Donal
Publication date	2017-11-15
Publication information	Andrade-Cabrera, Carlos, Daniel J. Burke, William J. N. Turner, and Donal Finn. "Ensemble Calibration of Lumped Parameter Retrofit Building Models Using Particle Swarm Optimization" 155 (November 15, 2017).
Publisher	Elsevier
Item record/more information	http://hdl.handle.net/10197/9117
Publisher's statement	This is the author's version of a work that was accepted for publication in Energy and Buildings. Changes resulting from the publishing process, such as peer review, editing, corrections, structural formatting, and other quality control mechanisms may not be reflected in this document. Changes may have been made to this work since it was submitted for publication. A definitive version was subsequently published in Energy and Buildings Volume 155, 15 November 2017, Pages 513-532 https://doi.org/10.1016/j.enbuild.2017.09.035
Publisher's version (DOI)	10.1016/j.enbuild.2017.09.035

Ensemble Calibration of Lumped Parameter Retrofit Building Models using Particle Swarm Optimization

Carlos Andrade-Cabrera[a], Daniel Burke[c], William J. N. Turner[b], Donal P. Finn[a,*]

[a]*School of Mechanical and Materials Engineering, University College Dublin, Belfield, Dublin 4, Ireland*
[b]*School of Electrical and Electronic Engineering, University College Dublin, Belfield, Dublin 4, Ireland*
[c]*Electrical Engineer, Warwick, UK*

Abstract

Simulation-based building retrofit analysis tools and electricity grid expansion planning tools are not readily compatible. Their integration is required for the combined study of building retrofit measures and electrified heating technologies using low carbon electricity generation. The direct coupling of these modelling frameworks requires the explicit mathematical representation of Energy Conservation Measures (ECMs) in building-to-grid energy system models. The current paper introduces an automated calibration methodology which describes retrofitted buildings as parametric functions of ECMs. The buildings are represented using a lumped parameter modelling framework. A baseline model, representative of the building prior to retrofit, and the retrofit functions are calibrated using Particle Swarm Optimisation. Synthetic temperature and heating load time-series data were generated using an EnergyPlus semi-detached house archetype model. The model is representative of this residential building category in Ireland. It is shown that the proposed methodology calibrates retrofitted building models to an acceptable level of accuracy (*MAE* below 0.5 °C). The methodologies introduced in the current paper are capable of generating lumped parameter building models with similar dynamics for different ECMs for any archetype building energy model. The identified building retrofit models have the potential to be integrated with electricity grid models in a computationally-efficient manner.

Keywords: Lumped parameter models, building model calibration, building retrofit, particle swarm optimization, integrated analysis.

Nomenclature

Variables and parameters

A	Area [m^2]
α	Calibration parameter (exponential approximation) [$-$]
β	Calibration parameter (exponential approximation) [$-$]
C	Lumped Capacitance [J/kgK]

d	Weather disturbances
ΔR	Variation in lumped resistance [$m^2 K/W$]
Δp	Variation in calibration parameters
ΔT_{avg}	Variation in annual average internal temperature [$°C$]
Δx	Variation in layer thickness increment [m]
$\mathcal{F}$	Set of fixed parameters (calibration)
$\mathcal{I}_n$	Set of thermal nodes adjacent to node n
$J(\cdot)$	Calibration cost function
g	Solar transmittance (Window) [$-$]
λ	Thermal conductance [W/mK]
M	Index for external insulation (Ensemble)
n	Number of insulation steps
nl	Number of layers in a wall
nC	Number of capacitances
nR	Number of resistances
N	Index for internal insulation (Ensemble)
NH	Calibration horizon [time steps]
O	Index for ceiling insulation (Ensemble)
p	Set of calibration parameters
Q	Heating Load [W]
R	Lumped Resistance [$m^2 K/W$]
T	Temperature [$°C$]
u	Heating load [W]
U	Thermal Transmittance (U-value) [$W/m^2 K$]
$\mathcal{V}$	Set of variable parameters (calibration)

Subscripts

0	Baseline model (Calibration parameters)
att	Attic
amb	Outdoor temperature
c	Ceiling node
$ceil$	Ceiling Insulation
$data$	Synthetic data
ext	External Insulation
gnd	Ground node

heat	Heat input	
int	Internal Insulation	
inf	Infiltration	
k	Time-step index (Building model thermal evolution)	
l	Time-step index (Particle Swarm Optimization)	
r	Room temperature	
M, N, O	Calibration parameter point (Ensemble)	
s	Solar gains	
si	Inside surface resistance [$m^2 K/W$]	
so	Outside surface resistance [$m^2 K/W$]	
wall	External walls	
win	Window	
theo	Theoretical value (resistance or capacitance)	
total	Total construction resistance	
w	Wall node	

Superscripts

★	Optimal (calibrated) parameter	

Acronyms

ACH	Air Changes per Hour	
BEMS	Building Energy Model Simulation	
CV(RMSE)	Coefficient of Variation of Root Mean Square Error	
ECM	Energy Conservation Measure	
EPS	Expanded polystyrene	
GA	Genetic Algorithm	
GAMS	General Algebraic Modeling System	
GHG	Greenhouse Gas (Emission)	
IWEC	International Weather Energy Conversion	
LP	Linear Program	
MAE	Mean Average Error	
MILP	Mixed Integer Linear Program	
MBE	Mean Biased Error	
PSO	Particle Swarm Optimization	
SEAI	Sustainable Energy Authority of Ireland	
SQP	Sequential Quadratic Programming	

1. Introduction

1.1. Decarbonisation of the residential sector in Ireland

Current European policy targets a reduction of greenhouse gas (GHG) emissions by at least 80% below 1990 levels by 2050, including a 95% abatement of GHG emissions in the building sector [1]. Buildings represent 40% of global energy consumption and account for nearly 30% of energy related global GHG emissions [2]. In the Irish context, the residential sector represents 25% of the primary energy supply [3] and a quarter of energy related CO_2 emissions in 2015 [4]. One approach to decarbonise the Irish residential sector using current technologies is the implementation of effective Energy Conservation Measures (ECMs), including upgrades of heating systems [5]. Ahern et al. [6] determined that building retrofit measures have the potential to reduce by 65% the heating costs and CO_2 emissions for detached rural houses built prior to 1979 (approximately 20% of the Irish domestic dwelling stock). Ahern et al. conclude that government incentives (such as the Better Energy Homes scheme [7]) are required to incentivise retrofit, given the significant upfront cost for end users. Without monetary or economic incentives, home owners are unlikely to carry out energy efficiency measures [8].

The Irish Government estimates an investment of 35 billion EUR (20,000 EUR per dwelling) is required to bring the domestic stock (as of 2015) to an efficient level of energy performance (BER rating B) [9]. There is a need for the study of techno-economic mechanisms by which the environmental and economic benefits of government investment in energy conservation measures are maximised. One such mechanism corresponds to the electrification of domestic space heating and domestic hot water supply. Under this mechanism, efficient electrified heating technologies such as heat pumps and storage heating [10] displace the CO_2 emissions arising from fossil fuel consumption for heating. The displaced CO_2 emissions are abated by the usage of low-carbon electricity generation assets. In 2015, fossil fuels accounted for 61% of energy-related CO_2 emissions in the residential sector [4]. During the same period, electricity accounted for only 25% of residential final energy use [3]. Furthermore, wind generation represents 23% of electricity generation and it is likely to increase in order to meet the Irish Government target of 40% generation using Renewable Energy sources [11]. Storage heating becomes a technology of interest as it has the potential to provide power system operators with demand management alternatives while increasing the usage of electricity generation assets [12].

The interconnection between building retrofits, electrified heating technologies and low-carbon electricity generation is evident. If energy efficiency measures and electrified heating systems are combined, the carbon emissions associated with domestic space heating and domestic hot water can potentially be displaced by low-carbon power generation. At an aggregated level, building and grid model integration has the potential to reduce peak electricity consumption and defer future investments in electricity generation capacity. Furthermore, heating storage can further minimize generation cost by shifting demand from excess wind production to domestic heat storage units. The integrated assessment of building retrofit measures, electrified heating technologies and variable energy generation requires the development of an integrated building-to-grid retrofit modelling framework by which the overall environmental and economic benefits can be maximised.

4

1.2. Modelling integrated building and grid retrofit policies

Techno-economic building retrofit optimisation often relies on the coupling of heuristic optimisation techniques (e.g., Genetic Algorithms) and Building Energy Model Simulation (BEMS) tools [13]-[16]. In such a framework, the heuristic optimisation solver uses BEMS models in an iterative manner for cost function evaluation purposes. However, power systems investment planning problems are often defined using classical optimisation models such as Mixed-Integer Linear Problems (MILP) (e.g.,[17] - [18]). Prior work that has addressed building-to-grid analysis focussed on methodologies that use BEMS and power systems optimisation in a sequential manner. This typically involves the use of BEMS to generate synthetic building performance data as an input to power systems optimisation tools. Ault et al. [19] adopted this approach by pre-calculation of heating demand profiles using the ESP-r simulation environment [20]. These heating profiles were used as input to a power systems optimization study.

A disadvantage associated with this approach is that BEMS are unable to adapt to dynamic events occurring in the power systems model (e.g., availability of variable generation or demand response events) unless a potentially sub-optimal iterative and computationally-expensive strategy is considered. For integrated energy scenario analysis, where building and grid models need to be combined, a linear representation of building energy performance is required. Integrated models of this nature will facilitate comprehensive building thermal performance assessment, such as building retrofit analysis or the effect of increased penetration of electrified space and water heating systems, in the context of wider integration of renewable energy generation into the electricity grid.

1.3. Contributions of this paper

The current paper introduces three automated calibration methodologies, each capable of transforming any residential BEMS archetype model into a lumped parameter archetype building model, representative of an ECM configuration. In the current paper, an *ECM configuration* is defined as a combination of ECM measures (e.g., 100 mm of external wall insulation combined with 200 mm of ceiling insulation). For any BEMS archetype, several ECM configurations can exist. The first methodology, denoted *Sequential Calibration*, exploits a semi-physical interpretation of the lumped parameter modelling framework, to define a selected building model parameter (e.g., external wall resistance), as a function of monotonic increments in an individual building fabric ECM (e.g., increments in external wall insulation thickness). These functions are defined as *retrofit functions*. To date, there has been no attempt to formulate lumped parameter building models automatically as functions of ECM. Sequential Calibration is constrained to the identification of a suitable *baseline* (i.e., pre-retrofit) lumped parameter building model. The second calibration methodology introduced in the current paper addresses this limitation by simultaneously identifying the baseline model and the retrofit function associated with each ECM. This methodology, denoted as *Simultaneous Calibration*, is shown to potentially result in a calibration bias (e.g., retrofitted models with low levels of insulation may be calibrated with less accuracy than the retrofitted models with higher levels of insulation).

The third methodology, which is the main contribution of the current paper, is denoted as *Ensemble Calibration*. The key difference is that Simultaneous Calibration defines a single retrofit function per ECM, whereas Ensemble

Calibration defines a group of retrofit functions, each one based on a combination of the other ECMs. For example, in Simultaneous Calibration there is only one single retrofit function associated with external wall insulation. In Ensemble Calibration, a retrofit function associated with external wall insulation is defined for every possible combination of ceiling insulation and internal insulation. Ensemble Calibration results in the identification of linear, lumped parameter models with a Mean Average Error (MAE) less than 0.5 °C, compared to the synthetic data generated using the associated BEMS archetype. This metric has been suggested in the literature as an acceptable calibration accuracy [21]-[23]. More importantly, the Ensemble Calibration methodology results in a number of lumped parameter building models with *shared* parameters (i.e., the baseline model). Therefore, the corresponding discrete-time linear building models are linearly dependent with respect to the discrete-time baseline model. This linearity is a key requirement of a building-to-grid co-optimization model used to assess optimal, large-scale ECM building configurations.

Ensemble Calibration is the first step towards the seamless integration of dynamic building energy models with grid models in an ECM investment decision-making framework. To date this broader agenda has not been addressed in the literature. The proposed methodology is not designed to support retrofit decision-making of an individual building retrofit project. Instead, the combinatorial archetype lumped parameter models developed using the proposed methodology have the potential to enable planners to simultaneously assess both ECM investment decisions and economic investment decisions when considering integrated building thermal and electricity grid flexibility analysis, which are usually considered at scale (e.g., at a national level). A case in point being that building retrofit policy-making (e.g., end-use incentives) can now be influenced by varying levels of RES penetration and/or electricity system investment options without the need to re-compute the building heating loads for each desired ECM configuration. Both the building thermal models and the power systems models could be simultaneously optimised, in theory, during the retrofit decision-making process.

The proposed framework does not explicitly deal with building model uncertainty at this stage of development. The explicit modelling of building uncertainty in linear archetype building models results in a non-linear model with varying parameters associated with uncertainty distributions for selected building parameters. This is not consistent with the desirable modelling framework for tractable building-to-grid co-optimisation (i.e., linear building modelling). To conclude, the methodologies introduced in the current paper assume the development of residential archetypes representative of a national building stock [24]. Residential archetypes are increasingly being used in building energy research at the urban and national level (e.g., [25]-[27]).The proposed contribution adds the possibility integrating power systems issues with urban and national energy modelling via BEMS archetypes, which to date has not been addressed.

1.4. Structure of the current paper

The current paper is organized as follows: Section 2 provides an overview of lumped parameter building modelling and model calibration via heuristics optimization. Section 3 describes methodologies to identify parametric evolution of a single ECM (Sequential Calibration) and multiple ECMs (Simultaneous Calibration). A third methodology

(Ensemble Calibration) is proposed to improve the accuracy of Simultaneous Calibration. Section 4 shows the application of these methods in the calibration of different lumped parameter models representative of an archetype of a semi-detached house model for all possible insulation retrofit combinations of external, internal and ceiling insulation. Section 5 provides a discussion of the results. Section 6 closes with the conclusions of the research work.

2. Background

2.1. Lumped parameter models

Simplified dynamic building energy models can be obtained from synthetic data using computing tools such as neural networks ([28]- [29]), support vector machines ([30, 31]) and machine-learning methods ([32]). Synthetic data can also be used to identify linear building models using linear regression ([33, 34]) and system identification methods ([35]). Alternatively, archetype construction information and synthetic data can be used for the calibration of lumped parameter building models ([36, 37]). The current work uses lumped parameter building models because of the intuitive semi-physical interpretation of the building model parameters.

Lumped parameter models (Figure 2) are a simplified representation of conductive and convective heat transfer through building elements. The approach is based on the electrical analogy method [38], in which electric resistances and capacitances model the thermal resistance and capacitance of material layers. The resulting multi-nodal model is further simplified by *lumping* parameters together, hence the name of the method. The heat balance at a thermal node n is modelled as a first order differential equation

$$C_n \frac{dT_n}{dt} = \sum_{\forall i \in \mathcal{I}_n} \frac{T_i - T_n}{R_i} + Q_n \tag{1}$$

where R_i is the thermal resistance between elements i and n, C_n is the thermal capacitance of the node, T_n represents the node temperature and Q_n models the heat fluxes applied to the node. The set $\mathcal{I}_n$ includes all nodes connected to node n. The resulting structure is often referred to as a 'thermal network'.

2.2. Lumped parameter model calibration

Building model calibration refers to the identification of unknown building energy model parameters based on metered or synthetic performance data. A detailed review of the calibration of such models is found in [39]. The current paper is concerned only with the automated calibration of deterministic lumped parameter models. Numerically, the automated calibration problem consists of identifying building model parameters which minimize the error between model predictions and synthetic or metered building data. The minimization problem is non-linear and non-convex given the nature of the parameters being estimated (e.g., $1/C_n R_i$). Gradient-based deterministic non-linear solvers such as Sequential Quadratic Programming (SQP) can be used only if a good initial point is provided [40] or if a large-multi-start approach is used [41]. Otherwise, the solution can be potentially attracted to local minima, which results in a sub-optimally calibrated model and therefore, less accurate energy predictions.

7

Stochastic building model calibration [42] is an approach that has gained acceptance among building modellers. The building dynamics are represented by stochastic differential equations and the parameters are identified via maximum likelihood estimation. The method is robust when noisy data sets are considered. Another possible approach is Bayesian Calibration ([43]). This method finds posterior distributions of uncertain building parameters given prior distribution assumptions. The approach performs well with noisy sensor data sets. These methods result in stochastic models (e.g., Kalman Filters) and statistical models (e.g., Gaussian emulators) which, while useful for other applications, are not compatible with a linear building-to-grid co-optimisation framework.

Another calibration approach is the use of heuristic optimization techniques. Such techniques do not require an initial point as an input parameter. However, there is no guarantee of global optimality, given the heuristic nature of the algorithm initialization. Furthermore, the method does not explicitly account for model uncertainties. Wang and Xu ([44]) use Genetic Algorithms (GA) to calibrate a heterogeneous building envelope and internal mass model using building data. The parameters of the building walls and roof, modelled as 3R2C (three resistances and two capacitances) networks, are identified via the minimization of the frequency response between the theoretical model and building performance. The internal mass is identified by minimizing the difference between the estimated and measured heating and cooling loads. Fraisse et al. [36] identified the parameters of a 4R5C model using GA and constant step tests on a logarithmic time scale, which account for fast and slow dynamics. Synthetic data was generated using an equation solver to generate simulated data.

All of the above mentioned calibration methods (stochastic, statistical and heuristic optimisation) focus on finding the parameters that calibrate a *single* building model. The aim of the current paper is to introduce methodologies which simultaneously calibrate *multiple* building models, where each model represents a possible ECM configuration of the same building. The current paper proposes three methodologies which define each possible retrofitted lumped parameter model as an explicit function of a baseline (uninsulated) building energy model and functions of single or multiple ECMs. It is shown that selected lumped model parameters (e.g., external resistance) can be modelled as exponential functions of the appropriate ECMs (e.g., external wall insulation thickness).

3. Methodology

3.1. Overview

The methodology framework is shown in Figure 1. The assumptions made for the generation of synthetic data and for lumped parameter building modelling are discussed in Subsection 3.2. Throughout the current paper, a single lumped parameter building model representative of an archetype model without any ECMs (i.e., a building before retrofit) will be referred to as the *baseline* model. Subsection 3.3 discusses the calibration of the baseline lumped parameter building model using synthetic data and Particle Swarm Optimization (PSO), a heuristic optimization technique. This method results in a linear state-space building model, which is numerically compatible with MILP electricity grid models. Due to the randomness of the PSO seed initialisation, the calibration of a linear state-space

8

building model separately for every ECM configuration will result in a baseline model and a number of retrofitted models with unrelated parameters. This implies that each retrofit model is required to be optimised independently, which is computationally expensive.

The current paper introduces Sequential Calibration (Subsection 3.4), which is a methodology that describes increments of a single ECM using only a baseline model and a parametric growth function. Using this method, some selected building model parameters are allowed to vary as the ECM increases (e.g., external wall resistance increases as external wall insulation thickness increases) while all the other parameters are fixed. This method results in parametric growth curves which can be approximated *a posteriori* using an exponential function approximation. Sequential Calibration is dependent on the baseline parameters, which may not satisfy the expected positive parameter growth (e.g., if the baseline parameter is identified at the upper parameter bound, such a parameter cannot have a positive growth). This difficulty is solved via Simultaneous Calibration (Subsection 3.5), which is a method that calibrates the baseline model and identifies exponential parametric growth functions for all ECMs at the same time.

It will be shown that Simultaneous Calibration can result in a calibration bias. For example, models with lower levels of insulation are calibrated with an inferior accuracy when compared to models with higher levels of insulation. Therefore, a third method, Ensemble Calibration (Subsection 3.6), is introduced to correct this inaccuracy. The difference between Simultaneous Calibration and Ensemble Calibration is that the exponential parameter growth functions identified via Simultaneous Calibration are independent of each other (e.g., the external insulation function is independent of the ceiling insulation function), whereas in Ensemble Calibration a parameter growth function of an ECM is identified for every possible combination of the other ECMs. These three methodologies are independent, so using one does not require the use of another.
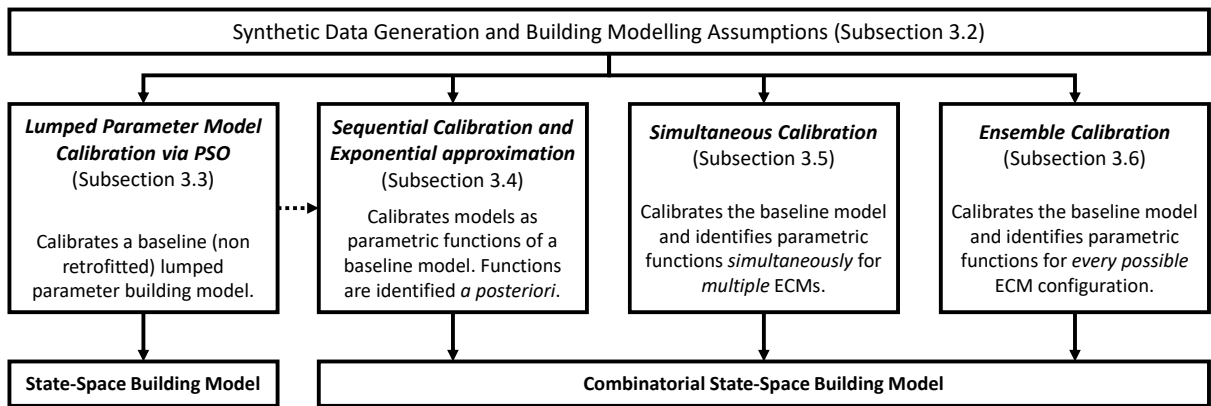

Figure 1: Overwiew of the proposed methodology

The calibration of individual building models (Subsection 3.3) results in a continuous-time lumped parameter model and a discrete-time state-space building model. The current paper identifies a continuous-time structure (baseline model and retrofit functions), which is denoted as an *Ensemble model*. The discretised Ensemble model results in

9

a combinatorial building energy model with shared dynamics (i.e., shared baseline parameters), which is potentially linearisable for integration in power systems models.

3.2. Synthetic data generation and building modelling assumptions

Synthetic data (namely, heating load time-series u_{data}, room temperature time-series $T_{r,data}$ and attic temperature time-series $T_{att,data}$) was generated using a BEMS semi-detached house building archetype model. This archetype is representative of double glazed ($U_{win} = 2.88\,[W/m^2K]$, $g_{win} = 0.759$), heavily built ($U_{wall} = 2.27\,[W/m^2K]$) two-storey houses, typically found in Ireland pre-1985 [24]. The dwelling features 10 thermal zones, each conditioned by electric radiators, as well as an unconditioned attic zone. The dwelling is modelled with a moderate infiltration rate (0.67 ACH per zone, 2.1 ACH in the attic). The weather data time-series d_{data} are extracted from the Dublin IWEC weather file [45]. Internal gains and mechanical ventilation losses are omitted during the synthetic data generation stage and during the calibration stage. The convective heating power time-series (Q_{heat}) is deemed to be a sufficient excitation signal to identify the required building envelope parameters [42]. Internal gains and ventilation losses can be latter added as convective heat inputs during the co-optimisation stage [46]. This simplification allows for the posterior implementation of internal gains and ventilation requirements associated with diverse occupancy patterns. The archetype will be deemed to be a protected building. The north and south façades cannot be altered and therefore they can only feature internal insulation. Furthermore, the west wall is modelled as adiabatic in order to emulate an adjacent dwelling. Therefore only the east wall can feature external insulation. Finally, ceiling insulation can also be included. This configuration allows for the study of simultaneous ECMs.

The proposed heterogeneous model topology is shown in Figure 2. Node T_{amb} represents the dry-bulb outdoor temperature. Nodes C_{w1} and C_{w2} and resistances R_{ext_1}, R_{ext_2} and R_{ext_3} model the two leaves of the external walls (as in [47]). The wall solar gains, $Q_{s,wall}$, are applied directly to node C_{w1}. C_r represents the capacitance of the air mass with room temperature T_r. Node C_{int} and resistance R_{int} model the thermal mass of the internal partitions and other slow dynamics (as in [48]). R_{win} represents the window thermal resistance. This resistance is the inverse of the window thermal transmittance U_{win}. The window solar gains $Q_{s,win}$ and the heating power input Q_{heat} are split between C_r and C_{int} via parameters f_1 and f_2. Node C_c and resistances R_{c_1} and R_{c_2} model the ceiling between C_r and the attic temperature node T_{att}. Finally, the node C_{gnd} and the resistances R_{gnd_1} and R_{gnd_2} model the heat transfer between the conditioned volume and the ground, as shown in [37]. T_{gnd}, the ground temperature below the conditioned space, is assumed constant at 18 °C, which is the default value used by EnergyPlus. Thermal bridges are not modelled in the current paper as they cannot be explicitly represented in the EnergyPlus building simulation environment. The accurate modelling of the thermal effects of thermal bridges would require an increased level of modelling effort both for the archetype model (e.g., 2D thermal simulation) and a modified lumped parameter model.

The synthetic data time-series were generated for the baseline model and all possible ECM configurations. External and internal insulation options were modelled as an additional expanded polystyrene (EPS) layer. Layer thicknesses have possible values of $[0, 100, 200, 300]\,mm$ for external insulation and $[0, 20, 40, 60]\,mm$ for internal insu-
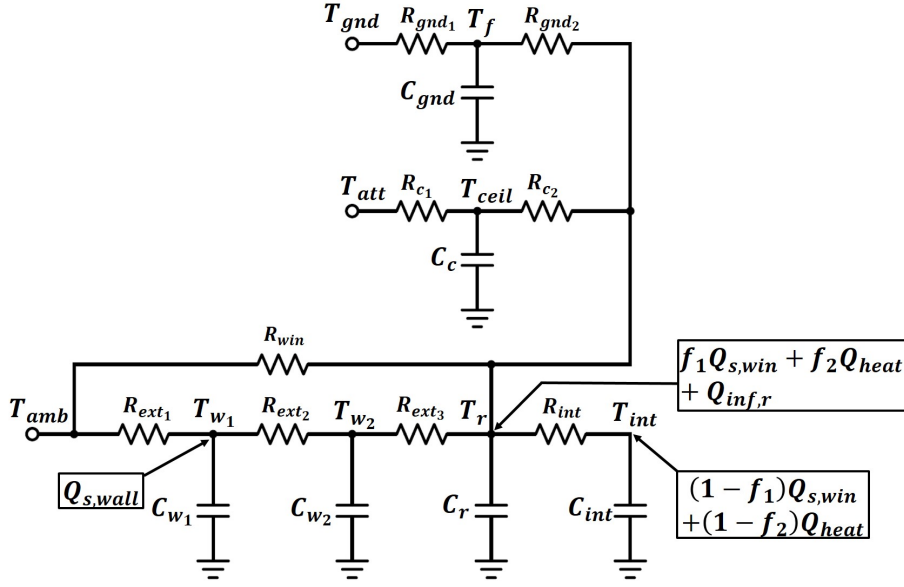
Figure 2: Proposed lumped parameter model topology (Semi-detached House)

lation. Ceiling insulation is modelled as a glass wool layer with possible thickness values of $[0, 100, 200, 300]\,mm$. The synthetic data time-series were generated for the heating season only (September 15th to March 15th). The same data is used for model calibration and performance evaluation, which implies that the metrics presented in this work should be considered as the best attainable performance. The model geometry, glazing thermal transmittance u_{value}, glazing solar transmittance and g_{value} and the infiltration rate ACH are extracted from the BEMS model.

As shown in [37] and [49], the continuous-time thermal network model and the heat transfer equations associated with external heat fluxes must be rearranged as a continuous-time state-space representation and then discretised for posterior numerical applications. Due to space limitations a full numerical model is not described in this paper.

3.3. Lumped parameter model calibration via particle swarm optimization

Particle Swarm Optimization (PSO) is a population-based algorithm in which candidate solutions, represented as particles with a given position and velocity, displace in a bounded space. Preliminary research ([50]) demonstrated that PSO can be used for the deterministic calibration of lumped parameter building models using EnergyPlus synthetic data from building energy archetypes. PSO becomes particularly useful when there is insufficient information required to obtain an accurate initial point for gradient-descent optimisation. The particle position of a candidate solution i is represented by the nR resistances and nC capacitances of the lumped parameter building model, that is

$$p(i) = [R_a\,(i, l)\quad R_b\,(i, l)\quad \ldots\quad R_{nR}\quad C_a\,(i, l)\quad C_b\,(i, l)\quad \ldots\quad C_{nC}] \tag{2}$$

with an assigned velocity vector $v\,(i, l)$ of identical dimensions. The index l represents the time-step (or function

11

evaluation count) of the PSO algorithm. The cost function of the particle is:

$$J\left(p\left(i,l\right)\right) = \frac{\displaystyle\sum_{k=0}^{k=NH} \sqrt{\left(T_{r,data,k} - T_{r,k}(i,l)\right)^2}}{NH} \tag{3}$$

where $T_{r,l}(i)$ is the temperature response of the model with the candidate solution parameters, and NH is the calibration horizon. At each time-step l, the PSO algorithm updates the velocities and positions of each particle based on their current position, the best historic position known to each particle and the position of the best particle in their neighbourhood. This procedure is repeated until a convergence criterion is reached. The candidate solution $p(i)$ which provides the least cost becomes the optimally calibrated set of parameters p. The reader is directed to [51] for a more detailed explanation of the algorithm. In this work, the PSO algorithm is deemed to have converged when the relative change in the optimal cost function at time-step l is less than 0.001 K during 20 consecutive iterations. Algorithm 1 describes the calibration algorithm for a single building model.

Algorithm 1: Building model calibration algorithm (single building model)

    Data: Candidate solution $p(i,l)$

    Result: Computed cost function of candidate solution i, $J(p(i,l))$

    Pre-Computed: Synthetic time-series $T_{r,data}$, u_{data}, d_{data};

    Known: Building geometry information;

    Assumptions: Glazing and infiltration properties: u_{value}, g_{value} and ACH;

    while *Convergence = False* **do**

        Extract $R_a, R_b, \ldots, C_n$ from $p(i,l)$;

        Calculate the continuous-time building model;

        Discretise the model and evaluate the particle cost $J(p(i,l))$ (Equation 3);

        Update $p(i)$ until convergence of the PSO optimisation solver ([51]);

    end

Since theoretical values can be computed using the building energy archetype model, every element of the particle position $p(i)$ can be re-defined as a multiplier of an associated theoretical thermal resistance and capacitance value. The particle position $p(i)$ becomes

$$p(i) = [p\left(i,l\right)_1 R_{1,theo} \ \ldots \ p\left(i,l\right)_{nR} R_{nR,theo} \ \ p\left(i,l\right)_{nR+1} C_{1,theo} \ \ldots \ p\left(i,l\right)_{nR+nC} C_{nC,theo}] \tag{4}$$

All particle positions associated with resistances were bounded between 0.1 and 10 [−] and all particle positions associated with capacitances were bounded between 1×10^{-2} and 1×10^2 [−]. The dimensionless factors f_1 and f_2 were bounded between 0.25 and 0.75. The theoretical thermal resistance and capacitance values used in the current

paper are defined in Appendix A.

Figure 3 shows the response of the calibrated model between December 1st and December 11th. A heating schedule with two heating windows was defined: one in the early morning (7AM to 9AM) and another in the evening (5PM to 11PM). The temperature set-point is deemed to be 21°C for living areas and 18°C for all other thermal zones. These set-points and schedules are representative of domestic heating requirements in Ireland ([52, 53]). An air capacitance multiplier of 11 was included in the EnergyPlus archetypes in order to represent realistic building behaviour [54]. Hence the room temperature may not reach the set-point.
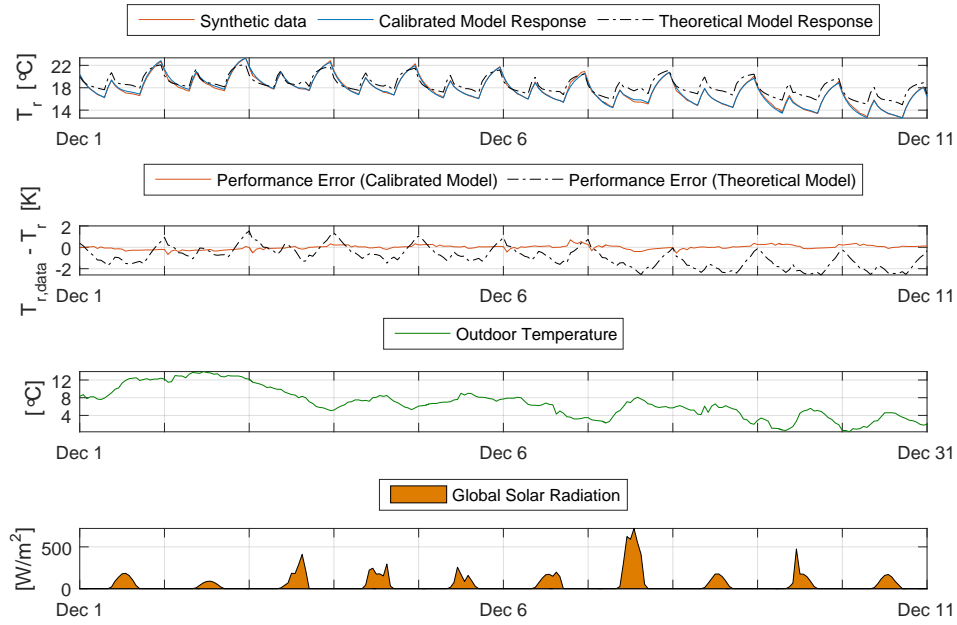
Figure 3: Temperature response of the calibrated model, Dec. 1st-11th

Three performance metrics were considered. The first is the Mean Absolute Error (MAE), which is the difference between the synthetic data and the model response [29]. The second metric is the Mean Biased Error (MBE, which signals whether a model underestimates (negative value) or overestimates (positive value) building response ([55]) The third metric is the Coefficient of Variation of the Root Mean Square Error ($CV(RMSE)$), commonly represented in the building modelling literature [55, 56]. ASHRAE Guideline 14-2000 [57] states that a model can be deemed as calibrated if the $CV(RMSE)$ deviates by less than 10% for annual metered energy data and 30% for hourly metered energy data. While this guideline applies to energy data, the metric serves as a guideline for temperature calibration accuracy.

The calibrated model estimates accurately the thermal response (MAE = 0.205 °C, $CV(RMSE)$ = 1.592%, MBE = −0.01%). The calibrated state-space building model was used on a heating load estimation routine implemented using the General Algebraic Modelling System (GAMS). The error in heating load estimation with respect

to the synthetic data was found to be 2.67%. Hence this particular model is deemed to be calibrated. Figure 3 also shows the response of the model prior to calibration (i.e., a model which uses the theoretical values described in Appendix A). The model response significantly deviates from the archetype model response (MAE = 1.437 °C, $CV(RMSE)$ = 10.09%, MBE = 7.393%). The error in heating load estimation increased significantly (37.17%). Hence the need for model calibration, despite the availability of theoretical estimates for model parameters.

3.4. Sequential calibration and exponential approximation

Figure 4 helps to visualize the nature of the problem that this research aims to address. Scenario (a) corresponds to the baseline (or uninsulated) case. The temperature evolution $T_{r,0}\left(p_0^\star\right)$ is the response of an optimally-calibrated model prior to any retrofit measures, $p_0^\star$. In scenario (b), an insulation layer of thickness Δx is added, which yields an average change in internal temperature $T_{r,\Delta x}\left(p_0^\star + \Delta p\right)$, assuming the same environmental conditions in both cases. The variation Δp is the *parametric evolution* between both scenarios. Since the initial PSO seed is randomized, and the optimization problem is non-convex, the independent calibration of these models will result in two different sets of calibration parameters.

a) $T_{r,0}(p_0^*)$ *b*) $T_{r,\Delta}(p_0^* + \Delta p)$ $T_{r,\Delta} > T_{r,0}$
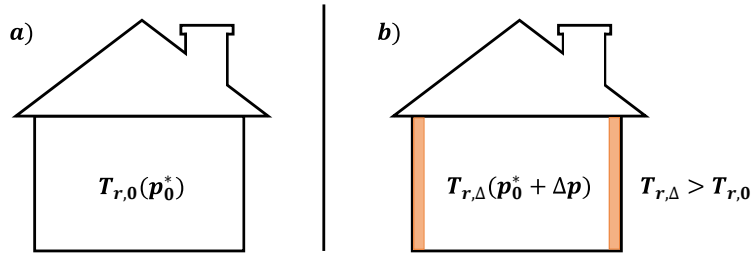
Figure 4: Increment in temperature due to increase in external insulation

Adding insulation results in an increment of the thermal resistance of a building element. The total resistance of a building element can be modelled as the sum of baseline calibration parameter $R_0^\star$ and the *parametric variations*

$$R_{total} \simeq R_0^\star + \{\Delta R_{ext}\left(\Delta x_{ext}\right), \ \Delta R_{int}\left(\Delta x_{int}\right), \ \Delta R_{ceil}\left(\Delta x_{ceil}\right)\} \tag{5}$$

$$C_{total} \simeq C_0^\star + \{\Delta C_{ext}\left(\Delta C_{ext}\right), \ \Delta C_{int}\left(\Delta C_{int}\right), \ \Delta R_{ceil}\left(\Delta C_{ceil}\right)\} \tag{6}$$

where ΔR_{ext}, ΔR_{int} and ΔR_{ceil} are the parametric variations in resistance due to thickness increments in external, internal and ceiling insulation (where appropriate). ΔC_{ext}, ΔC_{int} and ΔC_{ceil} are the parametric increments in capacitance due to thickness increments in external, internal and ceiling insulation (where appropriate). Theoretically, the capacitance of a building element may be altered due to the addition of material layers. For example, it is possible that building elements with low thermal capacitance are retrofitted with a thick layer of insulation. The current paper deals only with increments in thermal resistance as insulation is progressively added. The objective of this subsection

14

is to find a mechanism to automatically determine such variations in lumped parameter building models using BEMS synthetic data. This is exemplified by the study of the variation of external wall resistance R_{ext_1} as insulation is progressively added to the building. By semi-physical modelling, additions in external insulation are likely to modify R_{ext_1}. One alternative to overcome the randomness in PSO seed generation, and therefore isolate parameter evolution to a single parameter, consists of splitting the building model parameters between a set of variable parameters $\mathcal{V}$ (in this case R_{ext_1}) and fix the other building model parameters. The set of fixed parameters is denoted by $\mathcal{F}$. A locally optimal method to determine the evolution of R_{ext_1} as insulation increases consists of studying the parametric variation between insulation steps. For example, denote $R^{\star}_{ext_1, \Delta x_{ext}=10}$ as the optimal value of the external resistance when only 10 mm of external insulation has been added. $R^{\star}_{ext_1, \Delta x_{ext}=10}$ will be used as the initial point of the calibration problem which finds $R^{\star}_{ext_1, \Delta x_{ext}=20}$. This method is denoted as *Sequential Calibration*. A similar approach, introduced in [58] focuses on the real-time identification of lumped parameter models with respect to a baseline model in a temporal dimension, whereas the current paper is concerned with a physical dimension (e.g., insulation thickness).

This approach is demonstrated using the energy models detailed in Subsection 3.2. First, 31 sets of synthetic temperature time-series data were generated using the archetype model enhanced with an expanded polystyrene (EPS) layer with thickness varying between $[0-300]$ mm in 10 mm steps. A baseline model is then calibrated, using the procedure outlined in Subsection 3.3. The baseline model parameters $p_0^{\star} = \begin{bmatrix} R^{\star}_{ext_1,0} & R^{\star}_{ext_2,0} & \cdots & R_{nR} & C^{\star}_{w_1,0} & C^{\star}_{w_2,0} & \cdots & C_{nC} \end{bmatrix}$ are used as the initial point of the sequential approach. The procedure is outlined in Algorithm 2.

Algorithm 2: Sequential Calibration

    Data: Optimally calibrated baseline parameter $p_0^{\star}$ (Subsection 3.3)

    Result: Parametric evolution of $\mathcal{V}$: $\{R^{\star}_{ext_1, \Delta x_{ext}=10}, R^{\star}_{ext_1, \Delta x_{ext}=20}, \cdots R^{\star}_{ext_1, \Delta x_{ext}=300}\}$

    Pre-Computed: Synthetic time-series $T_{r,data}$, u_{data}, d_{data};

    Known: Building geometry information;

    Assumptions: Glazing and infiltration properties: u_{win}, g_{win} and ACH ;

    Initialisation: Define fixed parameters $\mathcal{F}$ and variable parameters $\mathcal{V} = \{R_{ext_1}\}$;

                   Define the initial point $R_{ext_1, \Delta x_{ext}=0}$ as $R^{\star}_{ext_1,0}$ from $p_0^{\star}$;

    for $k = 10 : 10 : 300$ **do**

        Call local optimisation routine with initial point $R_{ext_1, \Delta x_{ext}=k-10}$;

        while *Convergence = False* **do**

            Calculate the continuous-time building model with parameters $p = \{\mathcal{V}_{\Delta x_{ext}=k} = R_{ext_1, \Delta x_{ext}=k}, \mathcal{F}\}$;

            Discretise the model and evaluate the solution cost $J(p)$ (Equation 3);

            Update $R_{ext_1, \Delta x_{ext}=k}$ until convergence of the local optimisation solver;

        end

        Update $R_{ext_1, \Delta x_{ext}=k}$ with the optimal solution $R^{\star}_{ext_1, \Delta x_{ext}=k}$;

    end

Figure 5 shows that the parametric evolution of R_{ext_1} takes the shape of a curve, which was identified to be fourth order using the MATLAB Curve Fitting Toolbox [59]. The MATLAB function *fmincon*, which implements a Sequential Quadratic Programming (SQP) algorithm, was used as the local optimization solver.
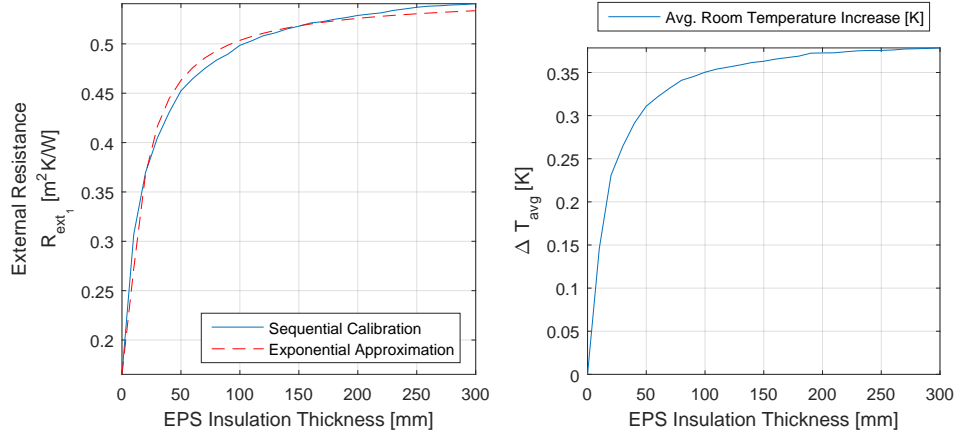

Figure 5: Exponential approximation of non-linear parametric evolution

This parametric evolution curve can be approximated with the exponential function

$$R_{ext_1,\Delta x_{ext}} \simeq R^{\star}_{ext_1,0} + \alpha_{ext}\, e^{\left(1 - \frac{\beta_{ext}}{\Delta x_{ext}/1000}\right)}, \qquad \Delta x_{ext} \geq 0 \tag{7}$$

where $R_{ext_1,\Delta x_{ext}}$ represents the value of R_{ext_1} at a given insulation Δx_{ext}, and α_{ext} and β_{ext} are the identified retrofit function parameters. For this particular example, $\alpha_{ext} = 0.141$ and $\beta_{ext} = 0.127$ were found using a parameter identification routine using IPOPT [60]. Figure 5 also shows that the parametric evolution is similar to $\Delta T_{avg,data}(\Delta x)$, the average increase in synthetic room temperature due to retrofit measures, defined as

$$\Delta T_{avg,data}(\Delta x) = \frac{\displaystyle\sum_{k=0}^{k=NH} T_{r,data,\Delta x,k} - T_{r,data,0,k}}{NH} \tag{8}$$

The intuition here is that large or small variations in average indoor air temperature difference will be reflected in large or small parametric adjustments, which results in the non-linear evolution of the parameters. The theoretical prediction for the total resistance of a multi-layered wall is defined ([40]) by the equation:

$$R_{total} = \frac{1}{A_{wall}}\left(r_{si} + r_{so} + \sum_{m=1}^{m=n_l} \frac{\Delta x_m}{\lambda_m}\right) \tag{9}$$

where r_{si}, r_{so} are inside and outside surface resistances and λ_m is the thermal conductance of a material layer m. By definition, monotonically positive increments in insulation thickness will result in monotonically positive linear

16

increments in R_{total} with a positive slope $\frac{1}{\lambda_{ins}}$, where λ_{ins} is the thermal conductance of the insulating material. In Sequential Calibration, however, this theoretical prediction holds true only for one dimensional heat transfer only. Figure 5 shows that the parametric evolution can be deemed to be linear for low levels of insulation (below 50 mm of EPS insulation thickness), which is aligned with the theoretical prediction. At high levels of insulation (above 150 mm of EPS insulation thickness) the parametric evolution saturates, which is in line with insulation saturation.

Figure 6 shows that the error-related performance metrics (i.e., MAE, $CV(RMSE)$) increase as insulation thickness increases, which implies that the baseline set of parameters $p_0^\star$ is not representative of highly insulated models. Thus, both the baseline parameters and the parameter growth (Equation 7) need to be identified simultaneously.
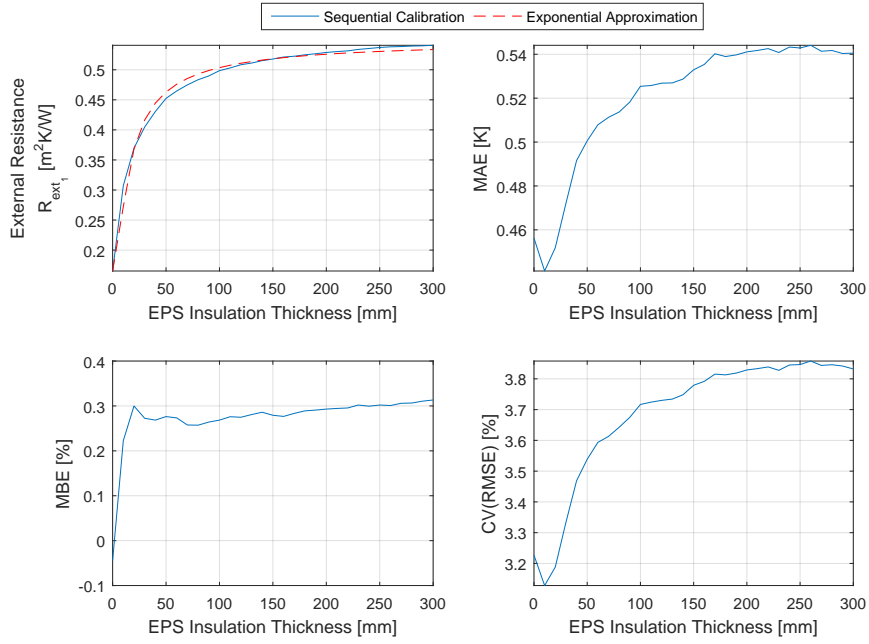
Figure 6: Exponential parameter approximation for external retrofit and error related performance metrics

3.5. Simultaneous calibration

Finding exponential parametric growth functions depends entirely on the selection of an appropriate baseline parameters $p_0^\star$. Furthermore, the retrofit function parameters α_{ext} and β_{ext} can only be identified *a posteriori*, which implies deviation in performance metrics 6). For incorrectly selected baseline parameters, the parametric growth could have a different behaviour (e.g., negative evolution), which is numerically feasible due to the local optimality nature of the method, but which lacks any meaningful physical sense (i.e., wall resistance values must increase as insulation increases). One approach to address this issue is to simultaneously calibrate the baseline parameters (Equation 4) and the parametric growth equation (Equation 7) for all of the ECMs. The method is denoted as *Simultaneous calibration*.

The calibration algorithm described in Algorithm 3 (Appendix B). The candidate solution $p(i, l)$ now includes the baseline model parameters and the calibration parameters α and β for each desired ECM. The upper and lower

17

parameter bounds for these parameters were defined as 2 and 0.001, respectively. In the current paper, the variable parameters $\mathcal{V}$ were selected as follows: The external wall resistance R_{ext_2} is affected by increments in external in-sulation, the internal wall resistance R_{ext_3} is affected by internal insulation and the external ceiling insulation R_{ceil_1} is affected by ceiling insulation. The selection criteria corresponds to a semi-physical modelling argument. In the lumped parameter building model framework, the selected parameters are most likely to be affected by the ECMs. The choice of R_{ext_2} over R_{ext_1} to model external insulation relates exclusively to calibration performance and will be explained in the results section. The candidate solution (i.e., particle position) $p(i)$ now includes the baseline parame-ters p_0 and the variable parameters $\mathcal{V}$. At each iteration l of the PSO solver, the global cost $J_{global}(p(i))$ is initialised. The global cost is the addition of the individual calibration performance (Equation 3). This global cost enables the algorithm to identify the baseline parameters and retrofit functions which simultaneously calibrate the baseline and all possible retrofitted models.

Define n_{ext}, n_{int} and n_{ceil} as the number of increments for external, internal and ceiling insulation, respectively. Define the indexes $M \in [1, n_{ext} + 1]$, $N \in [1, n_{int} + 1]$ and $O \in [1, n_{ceil} + 1]$ are increment indexes for the respective insulation directions. An index value of 1 represents that the baseline parameter is considered (i.e., the ECM has not been considered). For example, consider $n_{ext} = 4$. If the maximum external insulation thickness is 300 mm, each increment of M represents an increment of 100 mm of external insulation. When no external insulation is considered, then the index $M = 1$ and $R_{ext_1} = R^{\star}_{ext_1,0}$, regardless of N and O. This nomenclature allows to use a triad $\{N, M, O\}$ to define models at different levels of insulation. For each possible ECM configuration, the method calculates the performance of each modelled retrofit using the baseline parameters p_0 and the calculated values of the variable parameters $\mathcal{V}_{M,N,O}$.

Simultaneous Calibration defines, by design, the shape of the parametric growth, which has been identified in the previous section as exponential, but which could be of another nature under other modelling framework. Furthermore, the identification of each retrofit function is affected by the total calibration performance (i.e., global cost), which depends on the baseline parameters and the retrofit functions. Therefore, the method takes into account the calibration accuracy of mixed insulation models.

3.6. Ensemble calibration

Simultaneous Calibration identifies parametric evolution functions which take into account all possible ECM con-figurations. The method, however, assumes that a single parametric growth function (Equation 7) will be sufficiently representative of mixed insulated models which depend on other ECMs. For example, the parameters $R^{\star}_{ext_1}$ $\alpha^{\star}_{ext}$ and $\beta^{\star}_{ext}$ define the parametric evolution of external insulation (for $M = [1, 2, 3, 4]$) regardless of existing levels of internal insulation (e.g., $N = 4$, $O = 1$) or a combined internal and ceiling insulation (e.g., $N = 4$, $O = 4$). Due to the inherited inaccuracies of simplified linear modelling, it is possible that some retrofit functions may not be representative of all possible ECM configurations. This will lead to an inaccurate calibration and potentially to a calibration which is

biased.

One method to avoid such calibration bias (and thus increase accuracy for all models) is to model the parametric evolutions of an ECM as explicitly dependent on all the possible combinations of the other ECMs. In the previous example, two parametric growth functions of external insulation would now be identified using the parameters $\{\alpha_{N=4,O=1}\beta_{N=4,O=1}\}$ and $\{\alpha_{N=4,O=4}, \beta_{N=4,O=4}\}$. If the procedure is automated for every single possible ECM configuration, all models are likely to be more accurate, since the retrofit function is exclusive for an ECM configuration. The simultaneous calibration of a set of baseline parameters $p_0^\star$ and the parametric evolution functions of ECMs modelled as explicitly dependent on all possible combinations of the other ECMs is denoted as *Ensemble Calibration*. The method is described in Algorithm 4 (Appendix C). The fundamental difference with respect to the previous method (Algorithm 3) is the explicit definition of growth parameters which are dependent on the other ECMs (e.g, $\alpha_{ext_{N,O}}$, $\beta_{ext_{N,O}}$).

Ensemble Calibration results in a more accurate model at the expense of a larger dimensionality. For example: for external insulation, 16 piecewise calibration functions are identified ($n_{ext} \times n_{int}$), each one represented by two calibration parameters. Thus 32 variables need to be identified, in lieu of the 2 variables required in Simultaneous Calibration. Since all non-variable model parameters are shared via $\mathcal{F}$, Ensemble Calibration identifies a continuous-time structure which defines all the possible $n_{ext} \times n_{init} \times n_{ceil}$ retrofitted models as variations of the baseline model $p_0^\star$ and the parametric variations ($\mathcal{V}_{M,N,O}$). That is, the dynamics of all retrofitted models are related to the baseline model. The advantages of this property will be elaborated in the Discussion (Section 5).

4. Results

4.1. Simultaneous calibration

The Simultaneous Calibration methodology (Subsection 3.5) was applied to the semi-detached house archetype model (Subsection 3.2). Only four calibration steps (baseline model plus three insulation increments) were considered for each dimension. A higher resolution was deemed to be computationally too expensive. The baseline model was simultaneously calibrated with three exponential parametrisations, each representing an ECM, as outlined in Algorithm 3.3. Table 1 describes eight different ECM configurations that are considered in this document to analyse calibration performance. Test 1 corresponds to the baseline model (i.e., the building before retrofits). Tests 2-4 correspond to ECM configurations with a mix of internal and ceiling insulation. These tests are representative of dwellings where external insulation cannot be added due to aesthetic preferences or building regulations. In such a scenario, Tests 3 and 4 will be the more representative of building retrofit practice. Tests 5-8 corresponds to a mixture of ceiling insulation and a moderate level of external insulation (100 mm) before progressively adding internal insulation. In retrofit practice, Test 5 is most likely to be adopted due to economic considerations. The test cases were chosen to illustrate the effect of model inaccuracy due to calibration bias. Since the methods result in the identification

19

of parametric structures, which are functions of layer thickness, commercially-available levels of insulation (e.g., 150 mm of ceiling insulation) can be extracted with relative ease.

Table 1: Insulation Levels for each Test Case (in [*mm*])

Insulation	*Test 1*	*Test 2*	*Test 3*	*Test 4*	*Test 5*	*Test 6*	*Test 7*	*Test 8*
External (EPS) *[mm]*	0	0	0	0	100	100	100	100
Internal (EPS) *[mm]*	0	40	80	120	0	40	80	120
Ceiling (Glass wool) *[mm]*	0	300	300	300	300	300	300	300

Table 2 summarizes the performance of this calibration method for all the test cases. The Simultaneous Calibration algorithm slightly overestimates the synthetic data (positive *MBE* value) in the baseline model (Test 1) and considerably underestimates the synthetic data (negative *MBE* values) in Tests 3 and 4. The key performance metric (*MAE*) are outside of the acceptable accuracy range (*MAE* below 0.5 °C) for those test cases and therefore cannot be deemed as calibrated. The relatively poor calibration accuracy of Test 5 (*MAE* = 0.414 °C) is significantly higher than the good performance achieved in Tests 6-8 (e.g., *MAE* close to 0.2 °C, as per Subsection 3.3), even though the only variation is the progressive addition of internal insulation. This demonstrates the potential drawbacks of calibration bias in Simultaneous Calibration. Figures 7 and 8 compare the model response for the test cases with respect to the synthetic data. Figure 7 clearly shows the the model underestimation associated with Tests 3 and 4. These models will result in heating load underestimation. Likewise, Figure 8 shows the good calibration accuracy of Tests 6-8. Test 5, while still an acceptable calibration, presents an slight underestimation of the synthetic data.
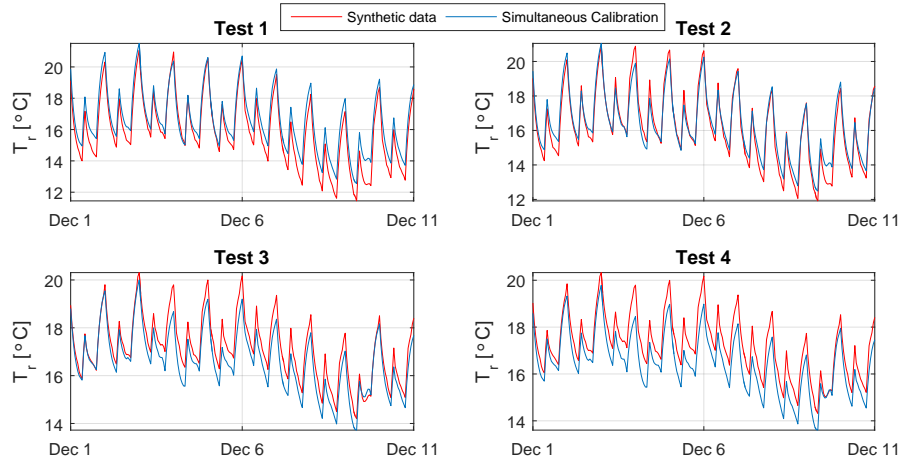

Figure 7: Model response for Tests 1-4 (Simultaneous Calibration)

Figures 9 and 10 show the histograms of the absolute error between the calibrated model response and the synthetic data at each time-step. A good calibration is represented by a distribution skewed towards the vertical axis (Tests 7 and 8 in Figure 10). The shape of the absolute error distributions for Tests 3 and 4 (Figure 9) can be interpreted as
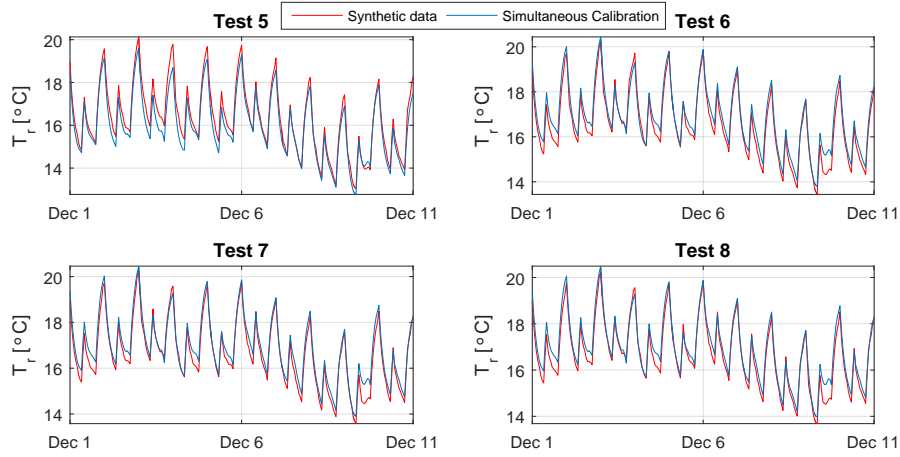
20

Figure 8: Model response for Tests 1-4 (Simultaneous Calibration)

Table 2: Performance Metrics: Simultaneous Calibration

Metric	Test 1	Test 2	Test 3	Test 4	Test 5	Test 6	Test 7	Test 8
MAE [°C]	0.574	0.421	0.730	0.968	0.414	0.272	0.249	0.2471
MBE [%]	2.893	-0.232	-4.046	-5.401	-1.804	0.798	0.261	0.1556
$CV(RMSE)$ [%]	4.165	3.140	4.738	5.918	2.911	2.008	1.801	1.7759

an error distribution around a persistent mean calibration error (bias). For Tests 3 and 4, the absolute errors can go
as high as 2.5 °C. The best performing models (Test cases 6-8) are calibrated below a maximum absolute error of
approximately 1 °C (Figure 10).
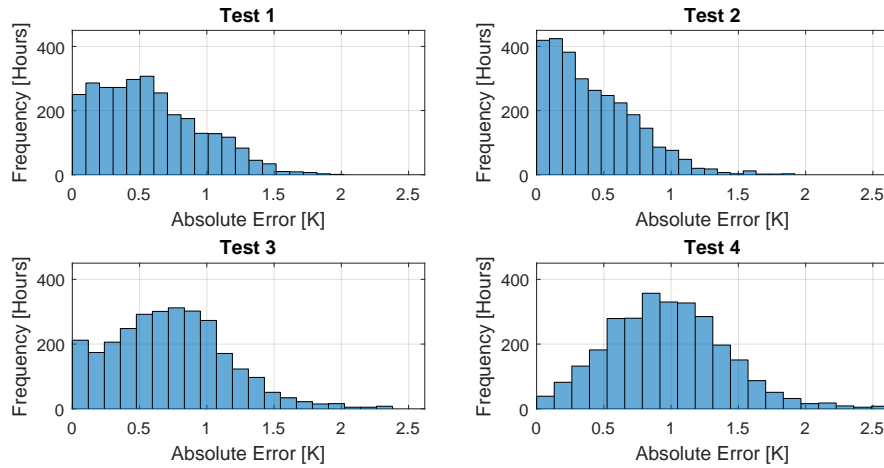
Figure 9: *MAE* histograms for Tests 1-4 (Simultaneous Calibration)

21
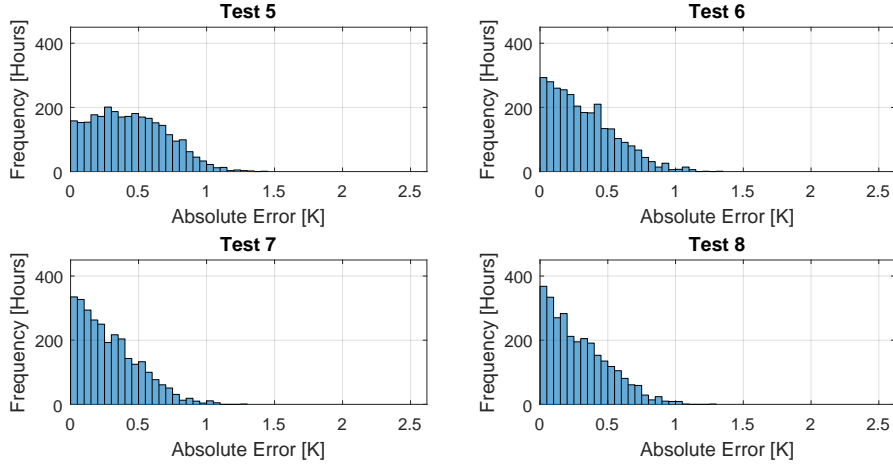
Figure 10: *MAE* histograms for Tests 5-8 (Simultaneous Calibration)

4.2. Ensemble calibration

The Ensemble Calibration method (Subsection 3.6) was applied to the archetype model using Algorithm 4. The Ensemble Calibration method reduces the global optimization cost ($J_{global} = RMSE_{avg} = 0.224°C$, compared to $J_{global} = 0.424°C$ for Simultaneous Calibration). This enhanced performance is clearly appreciated in the reduced *MAE* values of Tests 1, 3 and 4 when compared with respect to their performance using Simultaneous Calibration (Table 2). Most importantly, model underestimation/overestimation is considerably reduced for these test cases. The performance of Test 5 improves considerably (*MAE* = 0.218 °C in Ensemble calibration, *MAE* = 0.414 °C in Simultaneous Calibration). Such an improvement is not immediately translated to Tests 6-8, which were already at good performance levels (*MAE* values close to *MAE* = 0.2 in Table 2).

Table 3: Performance Metrics: Ensemble Calibration

Metric	*Test 1*	*Test 2*	*Test 3*	*Test 4*	*Test 5*	*Test 6*	*Test 7*	*Test 8*
MAE [°C]	0.317	0.350	0.266	0.278	0.218	0.190	0.195	0.201
MBE [%]	0.609	-0.630	0.247	-0.314	0.098	-0.021	-0.032	0.013
CV(RMSE) [%]	2.372	2.594	1.875	1.922	1.606	1.377	1.411	1.454

The improved calibration performance is noticeable in the model response shown in Figures 11 and 12. Noticeably, Tests 3 and 4 (Figure 11) do not present a persistent temperature underestimation (as in Figure 7), which is the key objective of the Ensemble Calibration methodology. All the test cases show an adequate match with respect to the synthetic data, particularly the mixed insulation ECM configurations (Tests 5-8). It is clear, however, that a slight calibration bias is still present in the baseline model (*MAE* = 0.31°C), which, while acceptable as calibration accuracy, is below the desirable value (*MAE* = 0.2°C), which is slightly noticeable when compared with the model response of Tests 5-8. Figure 13 shows that the *MAE* distributions for the ECM configurations with biased calibration (e.g.,

Tests 3-4 in Figure 9) are now skewed towards the vertical axis, which is a significant improvement. However, Tests 1 and 2 still show occasional error deviations up to 1.5 °C. At the same time, Figure 14 shows a very good calibration performance, with most of the model errors located below 0.5 °C. Therefore, Ensemble Calibration has shown a noticeable improvement in the reduction of calibration bias, but such bias is nonetheless persistent. This implies that further study on the mechanisms of bias reduction is required.
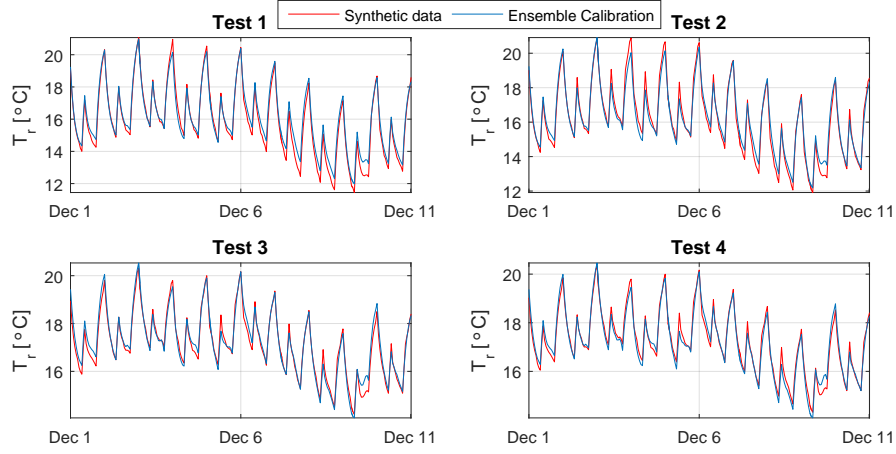
Figure 11: Model response for Tests 1-4 (Ensemble Calibration)
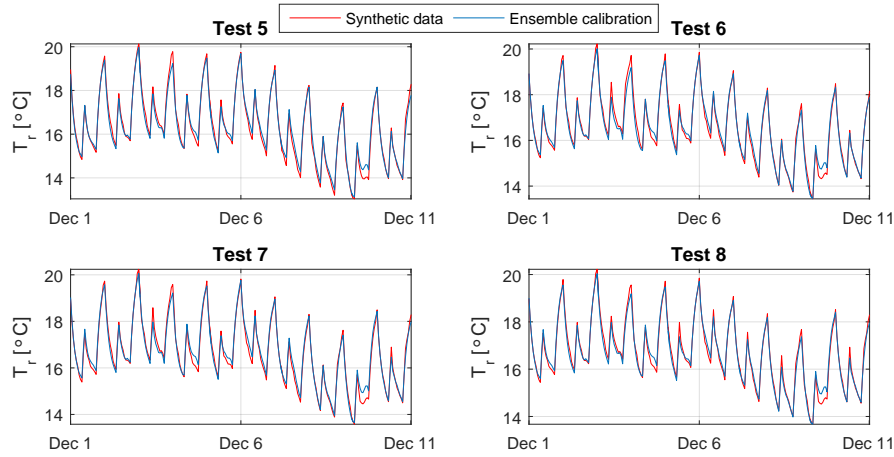
Figure 12: Model response for Tests 5-8 (Ensemble Calibration)

Figures 15 and 16 visualise such effect using *MAE* heat maps. The vertical axis represents the four possible values of external insulation (index M). The horizontal axis represents the four possible values of internal insulation (index N) at different values of ceiling insulation (index O). Each building energy model is represented by an element in the heat map. Every element is denoted by the index triad $\{M, N, O\}$, which describes its level of insulation,
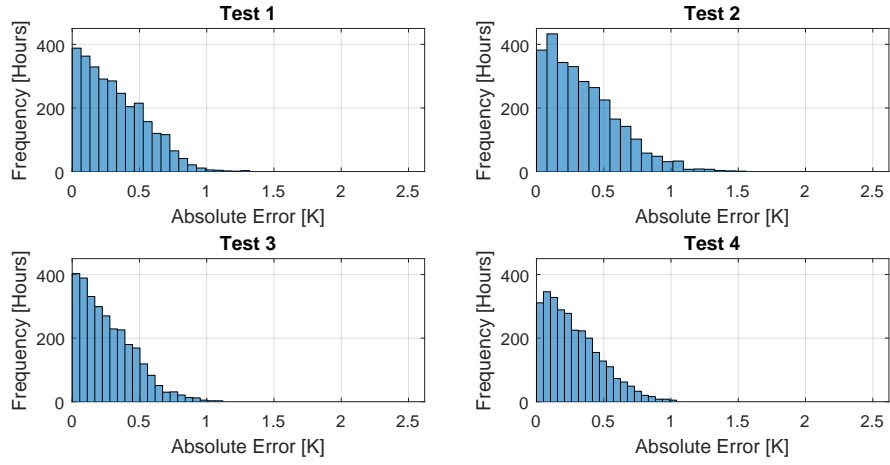
23

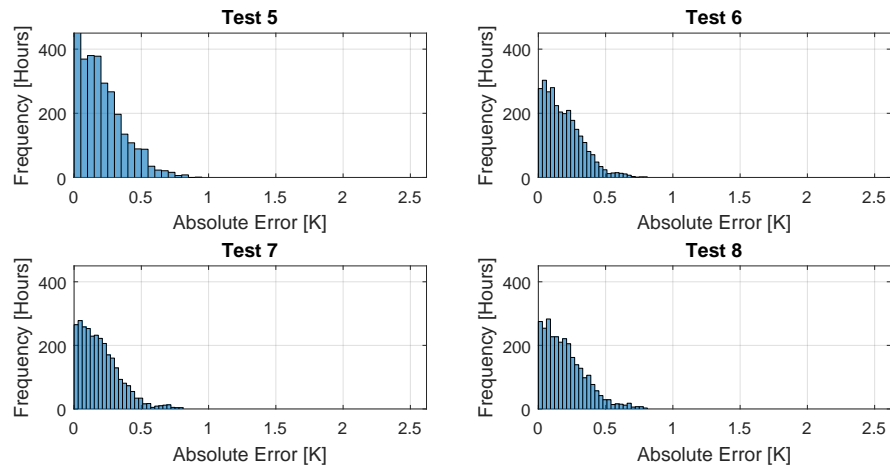Figure 13: *MAE* histograms for Tests 1-4 (Ensemble Calibration)

Figure 14: *MAE* histograms for Tests 5-8 (Ensemble Calibration)

and its performance using *MAE* as the key metric. Table 4 denotes the relationship between the indexes with the corresponding insulation thickness and the lumped model parameters affected by each ECM.

Table 4: Insulation Configuration for Ensemble Calibration Indexes (in [*mm*])

Index	Insulation	1	2	3	4	Parameter
M	External (EPS) *[mm]*	0	50	100	150	R_{ext_2}
N	Internal (EPS) *[mm]*	0	40	80	120	R_{ext_3}
O	Ceiling (Glass wool) *[mm]*	0	100	200	300	R_{ceil_1}

Figure 15 shows the *MAE* error distribution obtained with Simultaneous Calibration. The largest *MAE* values (in red) are clustered in the bottom row, which corresponds to progressive additions of ceiling insulation ($N = [1, 2, 3, 4]$) at all possible levels of ceiling insulation. This bias was illustrated in Tests 2-4. The bias is non-uniform. Without external insulation, progressive levels of internal insulation at maximum ceiling insulation ($O = 4$) result in an increased error (models $\{1, 1, 4\}$ to $\{1, 4, 4\}$, on the bottom corner). The same is not true for the cases once external insulation is added (e.g., models $\{3, 1, 4\}$ to $\{3, 4, 4\}$, which corresponds to Tests 5-8). In Ensemble Calibration (Figure 16), the error distribution is more uniform, but there still persist a residual calibration bias with respect to less insulated ECM configurations.
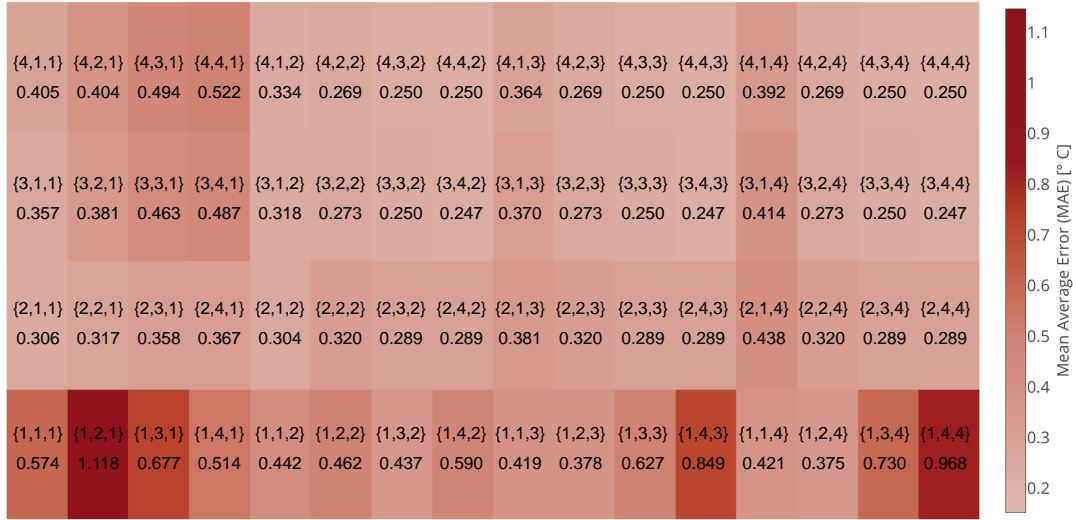

Figure 15: Mean Absolute Error (*MAE*) Heat Map (Simultaneous Calibration)

4.2.1. Parameter Selection

The results shown describe the best performance metric for each methodology under the variable parameter selection $\mathcal{V} = \{R_{ext_2}, R_{ext_3}, R_{ceil_1}\}$. The reason for this parameter selection is calibration performance. While semi-physical
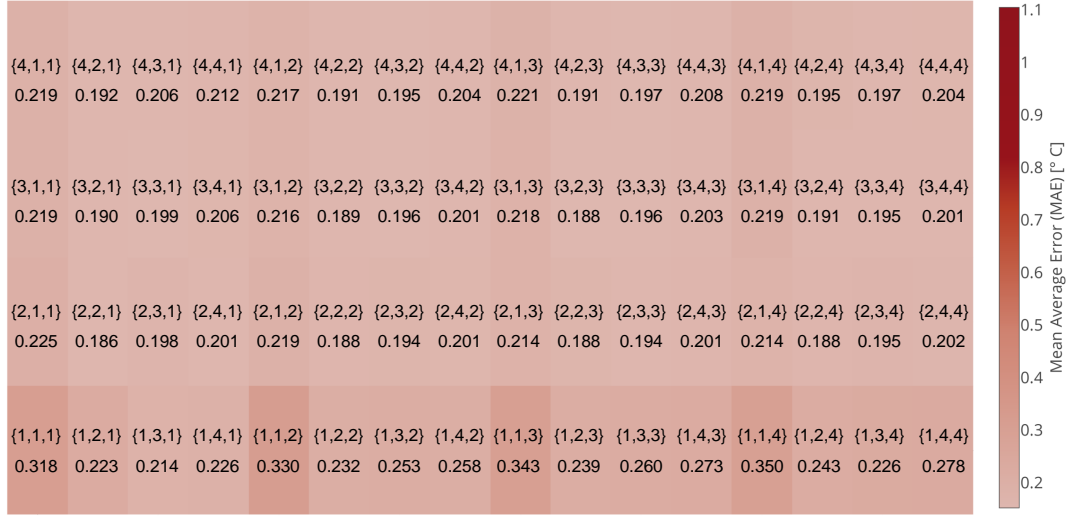
25

Figure 16: Mean Absolute Error (*MAE*) Heat Map (Ensemble Calibration)

modelling reasoning suggests that R_{ext_1} should be the parameter chosen, the resulting calibration accuracy is inferior with respect to the selection of R_{ext_2}. As mentioned earlier, Ensemble Calibration achieved $J_{global} = 0.224$ °C when R_{ext_2} was selected as the variable parameter. When R_{ext_1} is selected, the calculated global costs are $J_{global} = 0.574$ °C for Simultaneous Calibration and $J_{global} = 0.509$ °C for Ensemble Calibration. Figures 17 and 18 show the *MAE* heat maps correspond to the selection of R_{ext_1} as the variable parameter for Simultaneous Calibration and Ensemble Calibration, respectively. Note that a different scale is used to explain the behaviour of the calibration algorithms. Figure 17 shows that the Simultaneous Calibration algorithm results in a calibration bias towards less insulated elements (especially with respect to the models prior to external insulation, bottom row) and this bias is slightly improved by Ensemble Calibration (Figure 18), but the performance is ultimately inferior to Ensemble Calibration using R_{ext_2} as variable parameter (Figure 16).

A sensitivity analysis of the Ensemble model was run using the methodology proposed by Marino et al. [61]. The study tested the sensitivity of the Ensemble model to the potentially variable parameters (R_{ext_1}, R_{ext_2}, R_{ext_3}, R_{ceil_1} and R_{ceil_2}). The analysis showed that R_{ext_1} is the most sensitive parameter (partial rank correlation coefficient of 0.87) regardless of whether increments in external insulation were considered or not. Therefore, parametric variations in R_{ext_1} will have a significant impact on all the calibrated building models. Since the heuristic optimisation algorithm seeks to minimise the sum of individual errors, it will identify a baseline R_{ext_1} which is satisfactory for most models. This implies a design bias towards favouring mixed insulation models, which is exactly the behaviour that Ensemble Calibration seeks to avoid. Furthermore, the thermal performance of the retrofitted wall can be expressed as a series sum of thermal resistances, where the equivalent U-value of the combined wall becomes

$$U_{wall} = \frac{1}{(R_{\Delta_{ext}} + R_{ext_1}) + R_{ext_2} + R_{ext_3}} = \frac{1}{R_{ext_1} + (R_{\Delta_{ext}} + R_{ext_2}) + R_{ext_3}} \qquad (10)$$
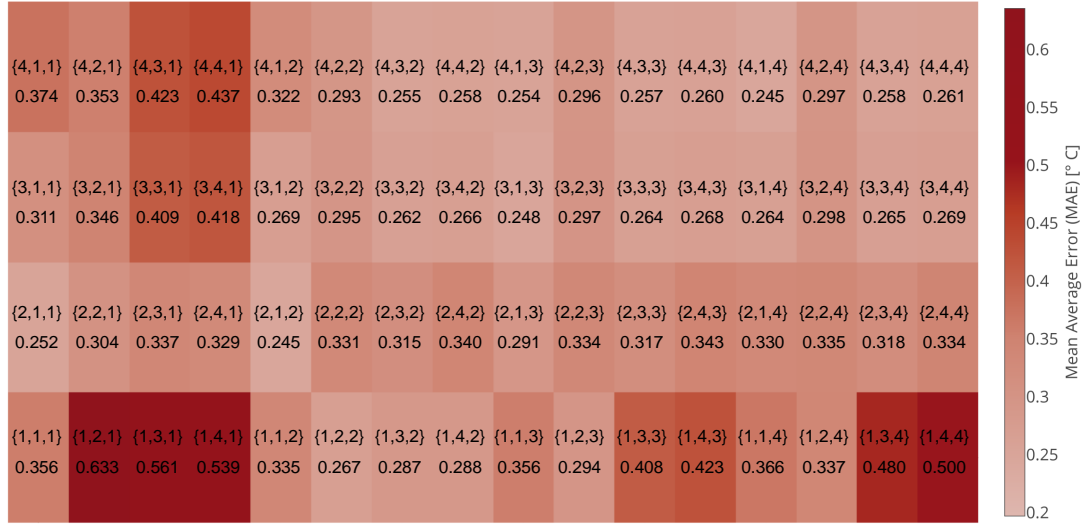
26

Figure 17: Mean Absolute Error (MAE) Heat Map, R_{ext_1} as variable parameter (Simultaneous Calibration)
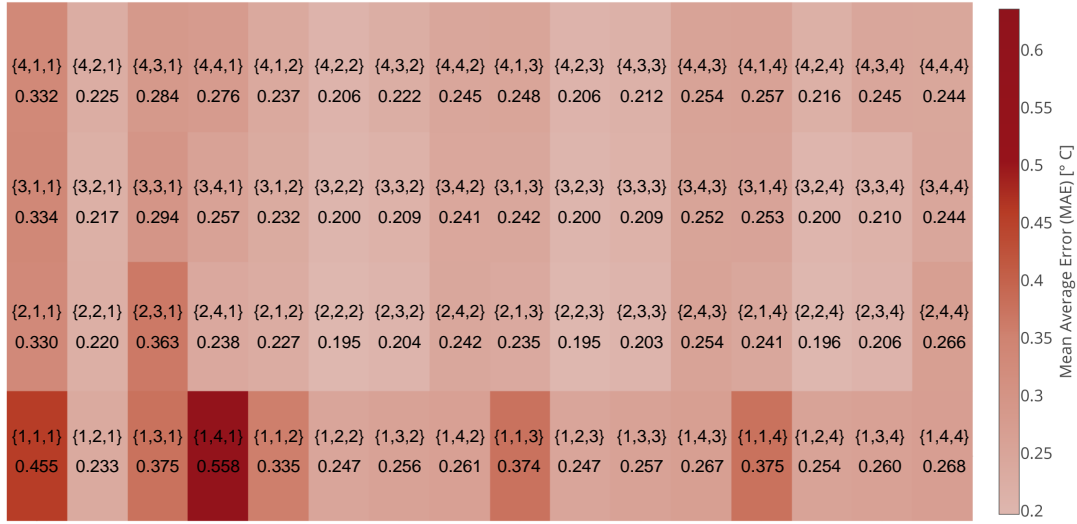

Figure 18: Mean Absolute Error (MAE) Heat Map, R_{ext_1} as variable parameter (Ensemble Calibration)

and therefore the desired thermal effect (parametric increment in total wall resistance) is achieved by shifting the expected parametric growth from R_{ext_1} to R_{ext_2}. Table 5 shows that using Ensemble Calibration with R_{ext_2} as the variable parameter provides the best average MAE_{avg} after 50 calibration runs. Table 5 shows the mean μ and standard deviation σ of the average MAE of all the calibrated models of a Simultaneous or Ensemble model. It is clear that the best performance is largely obtained by using Ensemble Calibration and R_{ext_2} as the variable parameter.

Table 5: Statistical significance of the results (50 runs)

Calibration	Variable	$\mu_{MAE_{avg}}$	$\sigma_{MAE_{avg}}$
Simultaneous	R_{ext_1}	0.386	0.081
Ensemble	R_{ext_1}	0.349	0.024
Simultaneous	R_{ext_2}	0.476	0.081
Ensemble	R_{ext_2}	0.284	0.043

5. Discussion

The three proposed calibration methodologies result in the identification of continuous-time Ensemble models. The Ensemble models consist of a baseline lumped parameter building model, which when combined with exponential functions, describe the variations in model parameters due to different ECM configurations. While it could be argued that extending a baseline model with theoretical approximations (e.g., Equation 9) or other simplified models should suffice, it is known that the theoretical model thermal performance may significantly differ from the more realistic BEMS building model performance (as shown in [50]). Hence the need to use automated calibration in order to identify lumped parameter building models representative of retrofitted BEMS archetypes. The proposed methodologies do not explicitly deal with building model uncertainty. However, such a study is feasible, if a parameter distribution (e.g., wall thermal transmittance U_{wall}) is associated with elements of the baseline lumped parameter model (e.g., R_{ext_1} - R_{ext_3}) in a stochastic optimization framework. Obtaining an Ensemble model using metered data in lieu of synthetic data is not feasible as this would require the acquisition of metered data sets (and therefore metered dwellings) for each ECM configuration under similar environmental conditions. On the other hand, the validation of the linear archetype building energy models identified via Ensemble calibration is feasible, provided that there exists an accurately calibrated pre-retrofit BEMS model of the dwelling for Ensemble calibration and that pre- and post-retrofit data are available. However, a physical validation of the proposed methodology is beyond the scope of the current paper.

The current paper introduces methodologies which model parametric growth due to ECMs in a lumped parameter building modelling framework. The advantage of the lumped parameter framework is the semi-physical interpretation of the model parameters. That is, there is a preliminary expectation of the model parameters that may vary when insulation is progressively added to a given building element. The modelling approach can be extended to other opaque construction measures (e.g., floor insulation, cavity wall insulation and roof insulation). However, window retrofits are not directly implementable in the current framework, as the building models are sensitive to large variations in the thermal transmittance parameter U_{win}. The inclusion of window retrofits is left for future study. The method can be adapted to other linear building modelling and identification frameworks (e.g., linear regression). The current paper has shown that the retrofit function can take the form of an exponential function. In the case of linear regression the question becomes one of identifying the regression coefficients affected by the ECMs while simultaneously identifying

the set of retrofit functions which fit the synthetic data best.

There is no strict need to use only one retrofit function per ECM. Consider the case of a building element with variable capacitance. The effect of the combined retrofit functions would be equivalent to fine tuning the product $\frac{1}{R_i C_i}$. This adjustment may prove numerically advantageous for calibration accuracy purposes. Note, however, that the modelling of additional retrofit functions does not guarantee a significant increment in calibration accuracy. Therefore, a trade-off must be reached between computational complexity and calibration accuracy. The methodologies introduced in the current paper form the basis of future studies on how the numerical interpretation of the lumped parameter framework may evolve in order to obtain the calibration of Ensemble building models.

Since the Ensemble model structure is functional, commercially-available values of insulation thickness not considered during the calibration process (e.g., 150 mm of ceiling insulation) can be extracted by means of a simple calculation (Equation 6) without the need for further model calibration. Furthermore, this study can be extended to more practical consideration (e.g., study of wall U-value targets) by means of altering the synthetic data generation methodology (i.e., optimise each archetype for target wall U-values, then proceed with Ensemble Calibration). It is also worth noting that while Simultaneous Calibration was not successful in calibrating ECM configurations with mixed insulation, it has other potential applications where a single building parameter is altered as a function of ECMs or other environmental conditions. Table 6 summarizes the advantages and disadvantages of the proposed automated calibration methodologies.

Finally, the numerical implementation of the Ensemble model is discussed. The thermal dynamics of a lumped parameter building model can be represented by state-space continuous-time models, which are discretised for numerical implementation [49]. These models are matrix representations of building thermal dynamics. The building models can be considered as a combinatorial model since all models are related to the baseline model. Furthermore, it is straightforward to identify the variation in dynamics due to building retrofits. It suffices to subtract the dynamics of a retrofitted building model from the dynamics of the baseline model. The advantage of such formulation is that the combinatorial retrofitted building models are potentially amenable to the simultaneous solution of cost-based building retrofit optimisation and heating load estimation via linearisation heuristics.

Future work will study the development of heuristic linearisation approaches for the solution of the combinatorial heating estimation problem. Likewise, other work will focus on the integration of building-to-grid models for retrofit investment planning studies from a wider European context. Further work efforts are also required in the explicit description of the shape of retrofit functions outside of the lumped parameter modelling framework. Finally, additional work is also required in the incorporation of other ECMs (e.g., glazing and air tightness) in Ensemble Calibration, as well as the propagation of building model uncertainty in Ensemble models.

29

Table 6: Summary of proposed calibration methodologies

Methodology	Advantages	Disadvantages
Lumped parameter model calibration via PSO (Subsection 3.3)	• Calibrates models to good accuracy levels ($MAE \leq 0\ 3°C$)	• Sensible to random PSO seed generation • Requires separate building-to-grid analysis for each ECM configuration
Sequential calibration and exponential approximation (Subsection 3.4)	• Fast (uses gradient-descent solvers)	• Requires adequate baseline parameters (e.g., not upper boundary) • May yield to negative parametric growth (unrealistic)
Simultaneous calibration (Subsection 3.5)	• Identifies baseline parameters adequate for parametric growth • Mixed insulation ECM configurations are explicitly considered • Suitable for single parameter variation	• Inaccurate with respect to individual calibration (Subsection 3.3) • Likely to present calibration bias
Ensemble calibration (Subsection 3.6)	• Improves model calibration accuracy with respect to Simultaneous Calibration • Reduces calibration bias • Functional structure (intermediate insulation values can be extracted)	• Computationally demanding • Slightly inaccurate with respect to individual calibration (Subsection 3.3)

6. Conclusions

The current paper introduced three calibration methodologies which aim to represent lumped parameter building models as mathematical functions of single or multiple ECMs (e.g., external wall insulation). The first methodology, Sequential Calibration, showed that lumped model parameter growth can be identified as an exponential function of monotonically increasing levels of an individual ECM (e.g., increments in external insulation layer thickness). The second methodology, Simultaneous Calibration, showed that both the baseline model calibration and the parameter growth function identification can be performed simultaneously for an individual ECM. It was shown that this calibration method is potentially biased when multiple ECM configurations are considered, given that the retrofit function for one ECM is identified independently of all possible combinations of the other ECMs. The third methodology, Ensemble Calibration, accurately calibrates all possible retrofit models by means of explicitly defining parameter growth functions of an ECM for every single combination of the other functions. This methodology results in an even distribution of individual model accuracy while requiring the identification of a larger number of calibration parameters. The methodologies introduced in the current paper generate lumped parameter models for different ECM configurations for any archetype building energy model. The generated lumped parameter models are numerically suitable for the integrated analysis of building retrofits and electricity grid models.

Acknowledgements

References

[1] European Climate Foundation, Roadmap 2050 A Practical Guide to a Prosperous, Low-carbon Europe, ECF, The Hague, Netherlands, 2010.

[2] United Nations Environment Programme, Climate Finance for Cities and Buildings: A Handbook for Local Governments, UNEP Division of Technology, Industry and Economics (DTIE), Paris, 2014.

[3] Sustainable Energy Authority Ireland, Energy in Ireland 1990 2015, SEAI, Dublin, Ireland, 2016.

[4] Sustainable Energy Authority Ireland, Energy-Related Emissions in Ireland - CO_2 Emissions from Fuel Combustion, SEAI, Dublin, Ireland, 2016.

[5] Sustainable Energy Authority Ireland, Energy Efficiency in Ireland, SEAI, Dublin, Ireland, 2016.

[6] C. Ahern, P. Griffiths, M. O'Flaherty, State of the Irish housing stock - Modelling the heat losses of Ireland's existing detached rural housing stock & estimating the benefit of thermal retrofit measures on this stock, Energy Policy 55 (2013) 139–151.

[7] M. Collins, J. Curtis, An examination of energy efficiency retrofit depth in Ireland, Energy and Buildings 127 (2016) 170–182.

[8] C. Aravena, A. Riquelme, E. Denny, Money, Comfort or Environment? Priorities and Determinants of Energy Efficiency Investments in Irish Households, Journal of Consumer Policy 39 (2) (2016) 159–186.

[9] Department of Communications, Energy and Natural Resources, Ireland's Transition to a Low Carbon Energy Future 2015-2030, DCENR, Dublin, Ireland, 2016.

[10] Energy Technologies Institute, Smart Systems and Heat: Decarbonising Heat for UK Homes, ETI, Birmingham, UK, 2015.

[11] EirGrid Group, All -Island Generation Capacity Statement 2016-2025, EirGrid, Dublin, 2016.

[12] K. MacLean, R. Sansom, T. Watson, R. Gross, Managing Heat System Decarbonisation: Comparing the impacts and costs of transitions in heat infrastructure, Imperial College Centre for Energy Policy and Technology, London, 2016.

[13] Z. Ma, P. Cooper, D. Daly, L. Ledo, Existing building retrofits: Methodology and state-of-the-art, Energy and Buildings 55 (2012) 889–902.

[14] E. Asadi, M. G. da Silva, C. H. Antunes, L. Dias, A multi-objective optimization model for building retrofit strategies using TRNSYS simulations, GenOpt and MATLAB, Building and Environment 56 (2012) 370–378.

[15] F. Ascione, N. Bianco, C. De Stasio, G. M. Mauro, G. P. Vanoli, A new methodology for cost-optimal analysis by means of the multi-objective optimization of building energy performance, Energy and Buildings 88 (2015) 78–90.

[16] G. M. Mauro, M. Hamdy, G. P. Vanoli, N. Bianco, J. L. M. Hensen, A new methodology for investigating the cost-optimality of energy retrofitting a building category, Energy and Buildings 107 (2015) 456–478.

[17] D. Pudjianto, M. Aunedi, P. Djapic, G. Strbac, Whole-systems assessment of the value of energy storage in low-carbon electricity systems, IEEE Transactions on Smart Grid 5 (2) (2014) 1098–1109.

31

[18] G. A. Bakirtzis, P. N. Biskas, V. Chatziathanasiou, Generation expansion planning by MILP considering mid-term scheduling decisions, Electric Power Systems Research 86 (2012) 98–112.

[19] G. Ault, J. Clarke, S. Gill, J. Hand, J. Kim, I. Kockar, K. Svehla, The use of simulation to optimise scheduling of domestic electric storage heating within smart grids, in: Proc. Building Simulation and Optimization (BSO2014), London, England, 2014.

[20] Energy Systems Research Unit, ESP-r software, University of Strathclyde, Glasgow, Scotland.

[21] X. Lu, T. Lu, M. Viljanen, Calibrating Numerical Model by Neural Networks: A Case Study for the Simulation of the Indoor Temperature of a Building, Energy Procedia 75 (2015) 1366–1372.

[22] X. He, Z. Zhang, A. Kusiak, Performance optimization of HVAC systems with computational intelligence algorithms, Energy and Buildings 81 (2014) 371–380.

[23] A. Kusiak, G. Xu, Modeling and optimization of HVAC systems using a dynamic neural network, Energy 42 (1) (2012) 241–250.

[24] O. Neu, S. Oxizidis, D. Flynn, F. Pallonetto, D. Finn, High resolution space - time data: Methodology for residential building simulation modelling, in: Proc. 13th International Building Performance Simulation Association Conference, Chambery, France, 2013 pp. 2428–2435.

[25] C. Cerezo, J. Sokol, C. Reinhart, A. Al-mumin, Three Methods for Characterizing Building Archetypes in Urban Energy Simulation: A Case Study in Kuwait City, in: Proc. 13th International Building Performance Simulation Association Conference, Hyderabad, India, 2015.

[26] P. Gianniou, A. Heller, P. S. Nielsen, K. Negendahl, Aggregation of building energy demands for city-scale models, in: Proc. 13th International Building Performance Simulation Association Conference, Hyderabad, India, 2015.

[27] D. Jermyn, R. Richman, A process for developing deep energy retrofit strategies for single-family housing typologies: Three Toronto case studies, Energy and Buildings 116 (2016) 522–534.

[28] A. H. Neto, F. A. Sanzovo-Fiorelli, Comparison between detailed model simulation and artificial neural network for forecasting building energy consumption, Energy and Buildings 40 (12) (2008) 2169–2176.

[29] G. Mustafaraj, G. Lowry, J. Chen, Prediction of room temperature and relative humidity by autoregressive linear and nonlinear neural network models for an open office, Energy and Buildings 43 (6) (2011) 1452–1460.

[30] B. Dong, C. Cao, S. E. Lee, Applying support vector machines to predict building energy consumption in tropical region, Energy and Buildings 37 (5) (2005) 545–553.

[31] Q. Li, Q. Meng, J. Cai, H. Yoshino, A. Mochida, Applying support vector machine to predict hourly cooling load in the building, Applied Energy 86 (10) (2009) 2249–2256.

[32] M. Brown, C. Barrington-Leigh, Z. Brown, Kernel regression for real-time building energy analysis, Journal of Building Performance Simulation 5 (4) (2012) 263–276.

[33] T. Catalina, J. Virgone, E. Blanco, Development and validation of regression models to predict monthly heating demand for residential buildings, Energy and Buildings 40 (10) (2008) 1825–1832.

[34] K. Yun, R. Luck, P. J. Mago, H. Cho, Building hourly thermal load prediction using an indexed ARX model, Energy and Buildings 54 (2012) 225–233.

[35] S. Prívara, J. Cigler, Z. Váňa, F. Oldewurtel, C. Sagerschnig, E. Žáčeková, Building modeling as a crucial part for building predictive control, Energy and Buildings 56 (2013) 8–22.

[36] G. Fraisse, B. Souyri, S. Pinard, C. Ménézo, Identification of Equivalent Thermal Rc Network Models Based on Step Response and Genetic Algorithms, in: Proc. 12th International Building Performance Simulation Association Conference, Sydney, Australia, 2011.

[37] I. Hazyuk, C. Ghiaus, D. Penhouet, Optimal temperature control of intermittently heated buildings using Model Predictive Control: Part I Building modeling, Building and Environment 51 (2012) 379–387.

[38] A. F. Robertson, D. Gross, An Electrical-Analog Method for Transient Heat-Flow Analysis, Journal of Research of the National Bureau of Standards 61 (2) (1958) 105–115.

[39] D. Coakley, P. Raftery, M. Keane, A review of methods to match building energy simulation models to measured data, Renewable and Sustainable Energy Reviews 37 (2014) 123–141.

[40] M. Gouda, S. Danaher, C. Underwood, Building thermal model reduction using nonlinear constrained optimization, Building and Environ-

ment 37 (12) (2002) 1255–1265.

[41] G. S. Pavlak, A. R. Florita, G. P. Henze, B. Rajagopalan, Comparison of Traditional and Bayesian Calibration Techniques for Gray-Box Modeling, Journal of Architectural Engineering 20 (2) (2014) 04013011.

[42] P. Bacher, H. Madsen, Identifying suitable models for the heat dynamics of buildings, Energy and Buildings 43 (7) (2011) 1511–1522.

[43] Y. Heo, G. Augenbroe, D. Graziano, R. T. Muehleisen, L. Guzowski, Scalable methodology for large scale building energy improvement: Relevance of calibration in model-based retrofit analysis, Building and Environment 87 (2014) 342–350.

[44] S. Wang, X. Xu, Simplified building model for transient thermal performance estimation using GA-based parameter identification, International Journal of Thermal Sciences 45 (4) (2006) 419–432.

[45] ASHRAE, International Weather for Energy Calculations (IWEC Weather Files) Users Manual and CD-ROM, Tech. rep., ASHRAE, Atlanta (2001).

[46] J. Terés-Zubiaga, C. Escudero, C. García-Gafaro, J. M. Sala, Methodology for evaluating the energy renovation effects on the thermal performance of social housing buildings: Monitoring study and grey box model development, Energy and Buildings 102 (2015) 390–405.

[47] A. Tindale, Third-order lumped-parameter simulation method, Building Services Engineering Research and Technology 14 (3) (1993) 87–97.

[48] Y. Ma, S. Richter, F. Borelli, Distributed Model Predictive Control for Building Temperature Regulation, in: SIAM (Ed.), Control and Optimization with Differential-Algebraic Constraints, Vol. 28 of Advances in Design and Control, 2013, Ch. Chapter 16, pp. 232–5.

[49] N. Good, L. Zhang, A. Navarro-espinosa, P. Mancarella, High resolution modelling of multi-energy domestic demand profiles, Applied Energy 137 (2015) 193–210.

[50] C. Andrade-Cabrera, W. J. Turner, D. Burke, O. Neu, D. P. Finn, Lumped Parameter Building Model Calibration using Particle Swarm Optimization, in: Proc. 3rd Asia conference of International Building Performance Simulation Association (ASIM 2016), Jeju, South Korea (2016).

[51] Mathworks, MATLAB Global Optimization Toolbox: User's Guide, The Mathworks, 2015.

[52] Sustainable Energy Authority Ireland, Dwelling Energy Assessment Procedure (DEAP), SEAI, Dublin, Ireland, 2012.

[53] AECOM, Cost Optimal Calculations and Gap Analysis for recast EPBD for Residential Buildings, Department of the Environment, Community and Local Government, Dublin, Ireland, 2013.

[54] E. M. Greensfelder, G. P. Henze, C. Felsmann, An investigation of optimal control of passive building thermal storage with real time pricing, Journal of Building Performance Simulation 4 (2) (2011) 91–104.

[55] G. Mustafaraj, D. Marini, A. Costa, M. Keane, Model calibration for building energy efficiency simulation, Applied Energy 130 (2014) 72–85.

[56] O. T. Ogunsola, L. Song, Application of a simplified thermal network model for real-time thermal load estimation, Energy and Buildings 96 (2015) 309–318.

[57] American Society of Heating, Refrigerating and Air-Conditioning Engineers, ASHRAE Guideline 14: Measurement of energy and demand savings, ASHRAE, Atlanta, 2002.

[58] E. Á. Rodríguez Jara, F. J. Sánchez de la Flor, S. Álvarez Domínguez, J. L. Molina Félix, J. M. Salmerón Lissén, A new analytical approach for simplified thermal modelling of buildings: Self-Adjusting RC-network model, Energy and Buildings 130 (2016) 85–97.

[59] Mathworks, MATLAB Curve Fitting Toolbox: User's Guide, The Mathworks, 2016.

[60] A. Wachter, L. T. Biegler, On the Implementation of a Primal-Dual Interior Point Filter Line Search Algorithm for Large-Scale Nonlinear Programming, Vol. 106, 2006.

[61] S. Marino, I. B. Hogue, C. J. Ray, D. E. Kirschner, A methodology for performing global uncertainty and sensitivity analysis in systems biology, Journal of Theoretical Biology 254 (1) (2008) 178–196.

33

Appendix A: Theoretical Thermal Resistances and Capacitances

Table A1 describes the theoretical thermal resistance and capacitance values, according with the formulation described in[40], and using the material and geometry information from the semi-detached EnergyPlus archetype energy model described in [24].

Table A1: Theoretical Thermal Lumped Resistance and Capacitance per Construction

Construction	Lumped Resistance [m^2K/W]	Lumped Capacitance [J/kgK]
External Wall	$R_{ext,theo}$=0.5815	$C_{ext,theo} = 2.040 \times 10^7$
Ceiling	$R_{ceil,theo} = 2.135$	$C_{ceil,theo} = 1.716 \times 10^6$
Floor	$R_{gnd,theo} = 0.197$	$C_{gnd,theo} = 2.923 \times 10^7$
Internal Partitions	$R_{int,theo} = 0.3205$	$C_{int,theo} = 2.040 \times 10^7$

Table A2 describes the association between specific lumped model parameters (Figure 2) and the theoretical values (Table A1).

Table A2: Relationship between Lumped Model Parameters and Theoretical Values

Parameters	Baseline Parameter
$R_{ext_1,theo}, R_{ext_2,theo}, R_{ext_3,theo}$	$R_{ext,theo}/3$
$C_{w_1,theo}, C_{w_2,theo},$	$C_{ext,theo}/2$
$R_{ceil_1,theo}, R_{ceil_2,theo}$	$R_{ceil,theo}/2$
$R_{ceil_1,theo}, R_{ceil_2,theo}$	$C_{ceil,theo}/2$
$R_{gnd_1,theo}, R_{gnd_2,theo}$	$R_{gnd,theo}/2$
$C_{gnd_1,theo}, C_{gnd_2,theo}$	$C_{gnd,theo}/2$

Appendix B: Simultaneous Calibration Algorithm

Algorithm 3: Simultaneous Calibration

Result: Parametric evolution of $\mathcal{V}$: $\{R_{ext_2 N,M,O}^{\star}, R_{ext_3 N,M,O}^{\star}, \ldots, R_{ceil_1 N,M,O}^{\star}\}$

Pre-Computed: Synthetic time-series $T_{r,data}$, u_{data}, $T_{attic,data}$, d_{data};

Known: Building geometry information;

Assumptions: Glazing and infiltration properties: u_{win}, g_{win} and ACH ;

Initialisation: Define upper and lower boundaries for baseline model parameters p_0 ;

Define upper and lower boundaries for the growth parameters α_{ext}, β_{ext}, α_{int}, β_{int}, α_{ceil} and β_{ceil} ;

Define fixed parameters $\mathcal{F}$ and variable parameters $\mathcal{V} = \{R_{ext_2 N,M,O}, R_{ext_3 N,M,O}, R_{ceil_1 N,M,O}\}$;

Call the PSO routine with particles $p(i) = \{p_0(i), \mathcal{V}(i)\}$;

while *Convergence = False* **do**

    Initialise the global cost $J_{global}(p(i)) = 0$;

    for $M = 1 : n_{ext}$ **do**

        for $N = 1 : n_{int}$ **do**

            for $O = 1 : n_{ceil}$ **do**

                if $M > 1$ **then**

                    Calculate wall resistance ($R_{ext_2 N,M,O}$) with α_{ext} and β_{ext} (Equation 7);

                end

                if $N > 1$ **then**

                    Calculate internal wall resistance ($R_{ext_3 N,M,O}$) with α_{int} and β_{int} (Equation 7);

                end

                if $O > 1$ **then**

                    Calculate external ceiling resistance ($R_{ceil_1 N,M,O}$) with α_{ceil} and β_{ceil} (Equation 7);

                end

                Calculate the continuous-time building model with p_0 and $\mathcal{V}_{N,M,O}$;

                Discretise the model and evaluate the local solution cost $J_{local}(p_0, \mathcal{V}_{N,M,O})$ (Equation 3);

                Update the global solution cost $J_{global}(p(i)) = J_{global}(p(i)) + J_{local}(p_0, \mathcal{V}_{N,M,O})$;

            end

        end

    end

    Update $p(i)$ until convergence of the PSO optimisation solver ([51]);

end

Appendix C: Ensemble Calibration Algorithm

Algorithm 4: Ensemble Calibration

Result: Parametric evolution of $\mathcal{V}$: $\{R_{ext_2}{}^{\star}_{N,M,O}, R_{ext_3}{}^{\star}_{N,M,O}, \ldots, R_{ceil_1}{}^{\star}_{N,M,O}\}$

Pre-Computed: Synthetic time-series $T_{r,data}$, $T_{attic,data}$, u_{data}, d_{data};

Known: Building geometry information;

Assumptions: Glazing and infiltration properties: u_{win}, g_{win} and ACH;

Initialisation: Define upper and lower boundaries for baseline model parameters p_0;

Define upper and lower boundaries for the growth parameters $\alpha_{ext_{N,O}}$, $\beta_{ext_{N,O}}$, $\alpha_{int_{M,O}}$, $\beta_{int_{M,O}}$, $\alpha_{ceil_{N,M}}$ and $\beta_{ceil_{N,M}}$;

Define fixed parameters $\mathcal{F}$ and variable parameters $\mathcal{V} = \{R_{ext_2 N,M,O}, R_{ext_3 N,M,O}, R_{ceil_1 N,M,O}\}$;

Call the PSO routine with particles $p(i) = \{p_0(i), \mathcal{V}(i), \}$;

while *Convergence = False* **do**

    Initialise the global cost $J_{global}(p(i)) = 0$;

    for $M = 1 : n_{ext}$ **do**

        for $N = 1 : n_{int}$ **do**

            for $O = 1 : n_{ceil}$ **do**

                if $M > 1$ **then**

                    Calculate wall resistance ($R_{ext_2 N,M,O}$) with $\alpha_{ext_{N,O}}$ and $\beta_{ext_{N,O}}$ (Equation 7);

                end

                if $N > 1$ **then**

                    Calculate internal wall resistance ($R_{ext_3 N,M,O}$) with $\alpha_{int_{M,O}}$ and $\beta_{int_{M,O}}$ (Equation 7);

                end

                if $O > 1$ **then**

                    Calculate external ceiling resistance ($R_{ceil_1 N,M,O}$) with $\alpha_{ceil_{N,M}}$ and $\beta_{ceil_{N,M}}$ (Equation 7);

                end

            Calculate the continuous-time building model with p_0 and $\mathcal{V}_{N,M,O}$;

            Discretise the model and evaluate the local solution cost $J_{local}(p_0, \mathcal{V}_{N,M,O})$ (Equation 3);

            Update the global solution cost $J_{global}(p(i)) = J_{global}(p(i)) + J_{local}(p_0, \mathcal{V}_{N,M,O})$;

            end

        end

    end

    Update $p(i)$ until convergence of the PSO optimisation solver ([51]);

end